# EFFECT OF TEMPERATURE AND AGEING ON THE ELECTRICAL BEHAVIOUR OF Al - Al$_2$O$_3$ - Al STRUCTURES

by

## KRISHNA   KUMAR   LAKHMANI
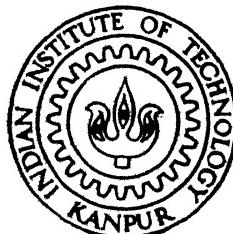
MATERIALS SCIENCE PROGRAMME

## INDIAN INSTITUTE OF TECHNOLOGY KANPUR

DECEMBER, 1996

# EFFECT OF TEMPERATURE AND AGEING ON THE ELECTRICAL BEHAVIOUR OF $Al-Al_2O_3-Al$ STRUCTURES

*A thesis submitted*

in Partial Fulfilment of the Requirements

for the Degree of

**MASTER OF TECHNOLOGY**

*by*

**KRISHNA KUMAR LAKHMANI**

*to the*

MATERIALS SCIENCE PROGRAMME

INDIAN INSTITUTE OF TECHNOLOGY, KANPUR

December, 1996

MSP - 1996 - M. LAK - EFF

# CERTIFICATE

It is certified that the work contained in the thesis entitled *"Effect of temperature and ageing on the electrical behaviour of $Al-Al_2O_3-Al$ structures"*, Mr. Krishna Kumar Lakhmani has been carried out under my supervision and that this work has not been submitted elsewhere for a degree.

December, 1996

Jitendra Kumar

(Jitendra Kumar)

Professor

Materials Science Programme

Indian Institute of Technology

Kanpur

# ACKNOWLEDGEMENTS

# DEDICATED

to

my Parents

# CONTENTS

# LIST OF FIGURES

# LIST OF TABLES

# ABSTRACT

The electrical behavior of metal-insulator-metal structures involving thin film technology continues to be the area of research interest due to their potential applications as charge storage capacitors, switching devices, cold cathode emitter, etc. They also have advantage of small weight, power saving, stability and rugged construction. Though extensive work has been undertaken on them in the past, yet, their nature and physical processes are not fully understood, principally, due to large number of variables involved. Also, investigations have been confined to measurements at room temperature. In order to understand their behavior better, the electrical behavior of $Al-Al_2O_3-Al$ have been studied at various temperatures. For this, $Al_2O_3$ is grown over vacuum evaporated aluminum films of thickness 2000 Å thermally in air at 50, 100, 150, 200°C. The top aluminum was deposited by thermal evaporation under vacuum ~ $10^{-6}$ torr using suitable masks to obtain various junctions having different areas (range 0.6-2.2 $mm^2$).

The analysis of current-voltage(J.V) data is shown to reveal the possible conduction mechanism(s) responsible for current flow as Ohmic, Schottky emission and field assisted tunneling in different voltage regimes at 25, 40 and 60°C. Also, Schottky emission and field assisted tunneling is found to get initiated at progressively lower voltages with increase in temperature. The barrier height obtained from the $ln(J)$ versus $V^{1/2}$ plots in

the linear region is shown to decrease with temperature; the value at room temperature being 0.70eV. Similarly, the field lowering coefficient ($\beta s$) increases with temperature. The capacitance of $Al$-$Al_2O_3$-$Al$ structure is found to decrease invariably with increase in temperature and is attributed mainly to the changes occurring in the interfacial characteristics. The rise in bulk capacitance that usually takes place with the rise of temperature is getting masked with the continuous decrease of the interfacial capacitance.

The breakdown of $Al_2O_3$ is shown to occur due to sudden increase in current beyond a certain voltage or through a forming process distinguished by voltage controlled negative resistance (VCNR) phenomenon. At this stage, the oxide turned conducting possibly due to creation of conducting channels in the bulk. Consequently, substantial heating takes place and $Al_2O_3$ becomes homogeneous by relieving the internal stress However, ageing of the $Al$-$Al_2O_3$-$Al$ structure displaying breakdown causes recovery of the insulating properties. These samples are shown to exhibit VCNR/ breakdown at much higher voltages. Such an observation is attributed to the resulting homogeneity and stability of $Al_2O_3$ during the previous breakdown cycle.

# CHAPTER - 1

## INTRODUCTION

Metal - insulator - metal (M-I-M) structures have received attention during the last three decades mainly due to their potential application as thin film devices, e.g.,switches, charge storage capacitors, cold cathode emitter,etc.[1,2]. These utilize thin film technology and have advantage of space, weight, power saving in addition to reliability, flexibility and low cost of design. However, exact nature of their electrical characteristics is not fully understood as yet. So, investigations regarding the passage of current through M-I-M structures and associated mechanisms are still relevant and continue to be the area of research activity. Of particular interest are the MIM structures comprising of thin insulating films like $SiO_2$, $Al_2O_3$, $Ta_2O_3$,etc. [3-11].

The conduction in insulators can take place due to thermal excitation of electrons and may be influenced by structural defects and impurities present. Due to the finite overlapping of wave functions of donor electrons, there can be hopping of carriers from one trap/impurity centre to another without going up into the conduction band. Consequently, an appreciable rise in current may occur if there are sufficient number of impurity centres in the bulk insulator. A very high electric field ($\sim 10^6$ V/cm) across the M-I-M structure causes drift

of electrons and ions through the thin insulating films and give rise to measurable currents. The actual behaviour is, however, influenced by thickness of oxide layer, interface barrier, temperature and nature of contacts and impurities, if present. Also, an anomalous behaviour involving permanent increase in the electrical conductivity is caused by the application of critical potential across the MIM structures. This is termed as forming process [12-15] and distinguished by a pronounced voltage controlled negative resistance (VCNR). The studies regarding the capacitance of such sandwiched structures have also been undertaken [16.17]. Nevertheless, investigations are restricted to measurement at room temperature. In order to understand the behaviour of M-I-M structures in-depth, it is indeed necessary to carry out current and capacitance measurements above room temperatures as well. An attempt has, therefore, been made here to study the I-V characteristics of Al-Al2O3-Al structures at various temperatures together with the accompanying variation in barrier height $(\phi)$ and Schottky barrier lowering coefficent $(\beta_s)$. Also, the effect of ageing on the current-voltage characteristics and temperature dependence of capacitance have been investigated.

## 1.1 Conduction mechanisms:

When low voltages are applied across a perfect insulator, no current flows. However, if the insulator is sufficiently thin and/or contains a large number of imperfections, a measurable amount of current results which depends on voltage, temperature

2

and oxide characteristics, etc. This current arises due to movement of electrons, holes and/or impurity ions. The nature of transport from one side to other is determined by the barrier formed at the electrode /insulator interface and/or the energy of traps present in the bulk. Accordingly, possible rate mechanisms are divided into two parts [13,18,19] :(a) barrier limited - tunneling, Schottky emission and thermionic field emission and (b) bulk limited - space charge, Poole-Frenkel effect, impurity conduction and internal field ionisation. All these are described below in brief and presented schematically in Fig.1.1.

### 1.1.1 Tunneling:

The concept of particle tunneling is very old now . Here the electron is represented by a quantum mechanical wave function and has a finite probability of tunneling through a reasonably thin potential barrier. On applying an electric field, electrons occupying states in one metal electrode of M-I-M structure tunnel through the insulator into the empty states on the other side and produce electronic current flow. A rectangular barrier model is generally used to calculate the tunneling current. although the exact shape depends on the image force, space charge, impurities present etc.

Simmons [20] evaluated the transmission coefficient for a general barrier of height $(\phi)$ and width $\Delta t$. The tunnel current density through a barrier of any arbitrary shape (Fig.1.2) at an applied voltage (V) at 0 K is given by

$$J = J_o\{\phi \exp (-A \ \phi^{1/2} ) - (\phi +eV)\exp[-A(\phi +eV)^{1/2} ]\} \qquad (1.1)$$

where $J_o = e/2\pi h(\Delta t)^2$, $A=(4\pi\Delta t/h)(2m)^{1/2}$, $\Delta t=t_2-t_1$ is the width of
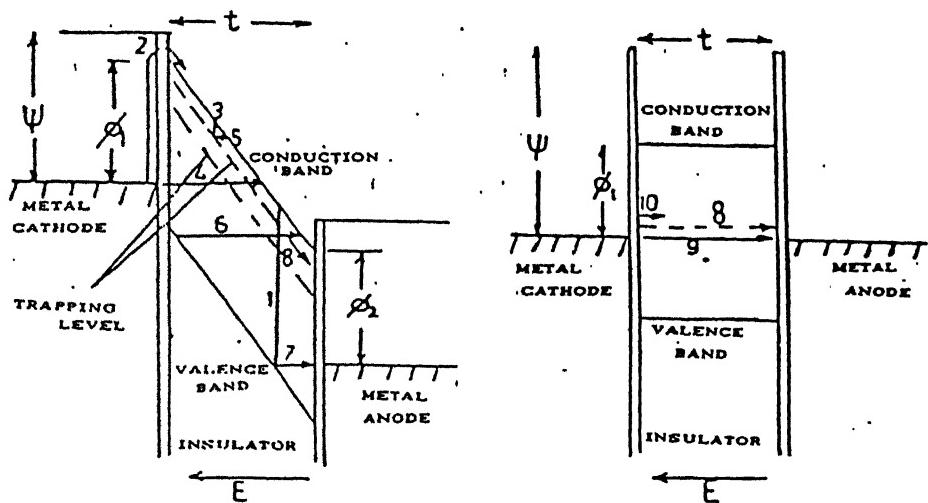
Fig 1.1    Schematic diagram of various conduction processes in

MIM structures

1)Electrons raised thermally from valence  band  if  band

gap is small and temperature is high;

2)Schottky emission from the metal;

3)Thermal excitation into the conduction  band  from  trap

levels in the insulators;

4)Tunneling from metal into the conduction band;

5)Tunneling from trap levels in the insulators;

6)Tunneling directly from valence band to conduction band;

7)Tunneling from valence  band  of  insulator  into  metal

electrode directly;

8)Ionic conduction;

9)Tunneling directly between two metal eletrodes;and

10)Impurity conduction.

$$J_0 \, \emptyset \, \exp(-A \, \emptyset^{1/2}) \longrightarrow$$

$$\longleftarrow J_0 \, (\emptyset + eV) \, \exp[-A(\emptyset + eV)^{1/2}]$$
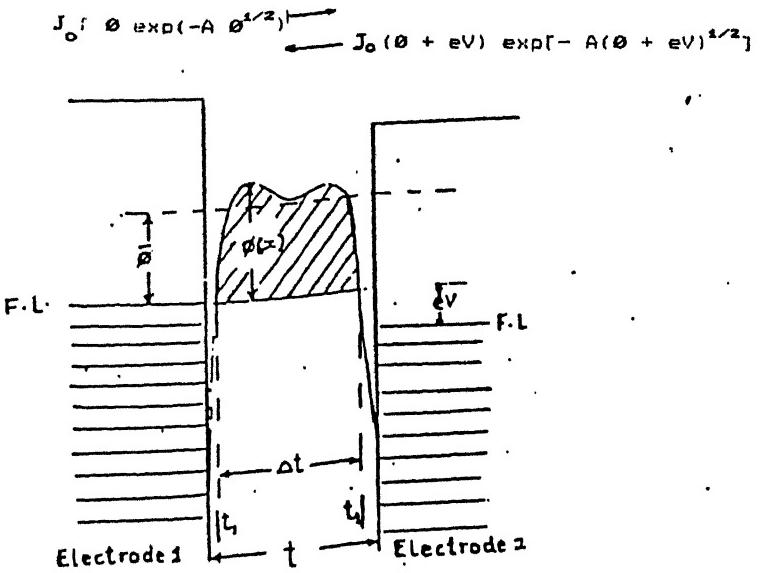
Fig. 1.2   Schematic diagram showing current flow between the electrodes for a generalised barrier

the barrier height at the Fermi level (Fig 1.2), $\phi$ is barrier height above Fermi level, h is the Planck's constant, e is the electronic charge, m is mass of electron and V is the applied voltage. For a rectangular barrier of height $\phi_0$, expression (1.1) leads to the following results.

(a) At low voltages (V  0), $\Delta t = t$, $\phi = \phi_0$

$$J = J_l \phi_0^{1/2} V \exp[-A \phi_0^{1/2}] \qquad (1.2)$$

Here $J_l = [(2m)^{1/2}/t](e/h)^2$ Thus, the current density has a linear bias dependence and the junction is ohmic at low voltages.

(b) At intermediate Voltages ( $V \leq \phi_0/e$ ), $\Delta t = t$, $\phi = (\phi_0 - eV/2)$

$$J = J_0 \{(\phi_0 - eV/2) \exp[-A(\phi_0 - eV/2)^{1/2}]$$
$$-(\phi_0 + eV/2) \exp[-A(\phi_0 + eV/2)^{1/2}] \} \qquad (1.3)$$

(c) At high Voltages (V $\geq \phi_0/e$), $\Delta t = t\phi_0/eV$, $\phi = \phi_0/2$

$$J = J_0 (2.2(eV)^2/4\phi_0)\{\exp[-2A \phi_0^{3/2}/(2.96eV)]$$
$$-(1+2eV/\phi_0)\exp[(-2A \phi_0^{3/2}/(2.96eV))(1+2eV/\phi_0)^{1/2}]\} \qquad (1.4)$$

where $J_0 = e/2\pi ht^2$ and $A = (4\pi t/h)(2m)^{1/2}$. Fig(1.3c) illustrates the energy band diagrams for the above three cases.

(d) At very high voltages ( V $\gg \phi_0/e$), above equation (1.4)reduces to Fowler – Nordheim form as second term is negligible. Thus,

$$J = J_0' \frac{2.2(eV^2)}{4 \phi_0} \exp[-\frac{2A \phi^{3/2}}{2.96 \ eV}] \qquad (1.5)$$

This situation is analogous to field emission from a metal electrode.It may be mentioned that the effect of image force is to round off the barrier corner such that height and width both get reduced (Fig 1.4). This causes increase in flow of current between the electrodes. In such cases the current density expressions get appropriately modified [20].

## 1.1.2 *Schottky emission:*

This involves emission of electrons from the metal (at negative potential ) to the insulator . This process is analogous to thermionic emission except that the applied electric field lowers the barrier height. Hence, electrons can escape easily to the conduction band of the insulator .The phenomenon is termed as Schottky emission. When electron is at a distance 'x ' away from the metal surface , it experiences a force [11,20-22]which is attractive in nature . As a consequence, the potential energy of the electron becomes

$$\phi = - \frac{e^2}{(16\pi\varepsilon_0 Kx)} \qquad (1.6)$$

where $\varepsilon_0$ is permittivity of free space and K is the dielectric constant of the medium . Then effective barrier height $\phi$ (x) with respect to the farm level is given by

$$\phi (x) = \phi_0 + \phi_{im} = \phi_0 - \frac{e^2}{16\pi\varepsilon_0 Kx} \qquad (1.7)$$

where $\phi_0$ is rectangular barrier height.The nature of $\phi(x)$ is shown in fig 1.5 . Schottky assumed that the image force holds only for x greater than some critical distance $x_0$ . For x<$x_0$, potential energy is linear function of x . When an electric field exists at metal-insulator surface , it interacts with image force and lowers the barrier. The line CD represents the potential due to uniform field . The resultant barrier potential $\phi'$(x) shown by dashed line RS in Fig(1.5), is given by

$$\phi'(x) = \phi_0 - \frac{e^2}{16\pi\varepsilon_0 Kx} - eEx \qquad (1.8)$$

Thus, the minimum decrease in barrier height ($\phi_0$) becomes

$$\Delta\phi_s = [\frac{e^3}{4K\pi\varepsilon_0}]^{1/2} (V/t)^{1/2} = e\beta_s V^{1/2} \qquad (1.9)$$

where E = V/t and $\beta_s = [\frac{e}{4\pi\varepsilon_0 K t}]^{1/2}$ . Now, the total current
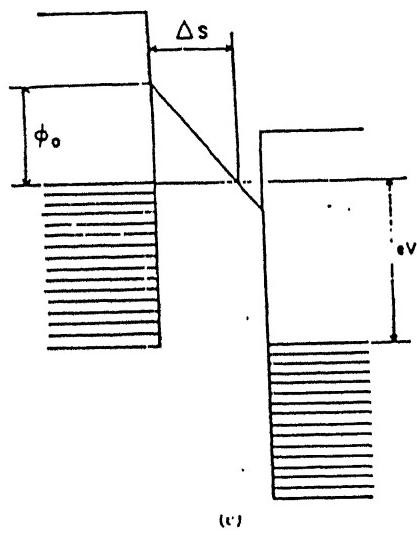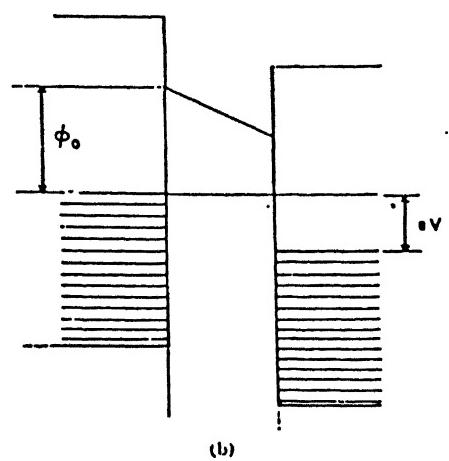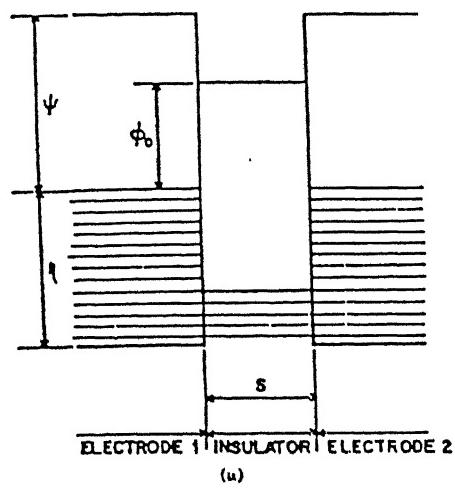
Fig.l3. Rectangular potential barrier in insulating film between metal electrodes for:
(a) $V = 0$; (b) $V < \varphi_0/e$; (c) $V > \varphi_0/e$.
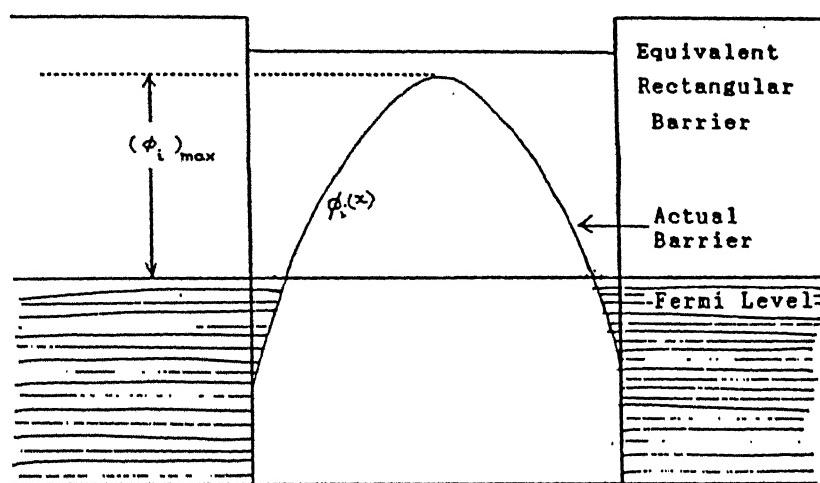
Fig 1.4 Energy diagram of a rectangular barrier with
image potential superimposed.

across the M-I-M structure is given by the Richardson - Schottky equation [11],

$$J = A^* T^2 \exp[-(\phi_o - \Delta\phi_s)/kT] \qquad (1.10)$$

or $\qquad J = A^* T^2 \exp(-\phi_o/kT) \exp(e\beta_s V^{1/2}/kT) \quad (1.11)$

where $A^* = 4\pi m e k^2/h^3$ is the Richardson-Dushman constant in units of Amp-cm$^{-2}$K$^{-2}$ . Thus ,Unlike the tunneling , Schottky emission current is temperature dependent . So the linear portion of ln (J) verses $V^{1/2}$ plot may correspond to Schottky emission. This effect was first observed in Al- $Al_2O_3$- Al structure by Emptage and Tantraporn [23]. Later Pollack [24] analyzed the temperature and voltage dependence of current and found the result in agreement with eqn (1.11).

### 1.1.3 *Poole-Frenkel effect:*

This is bulk analogous to Schottky emission and involves thermal excitation of electrons from trap or donor centres in to the conduction band of the insulator [12] The potential energy of the electron at a distance x away is just $-e^2/4\pi Kx$ where K is the dielectric constant of the insulator . It may be noted that this energy is four times to that resulting from the image force effects for the same distance x. Proceeding as before the Pole-Frenkel lowering of barrier (Fig.1.6)in a uniform field is

$$\Delta\phi_{pf} = (\frac{e^3}{\pi \varepsilon_0 K t})^{1/2} V^{1/2} = e\beta_{pf} V^{1/2} \qquad (1.12)$$

where $\beta_{pf} = (e/\pi\varepsilon_0 Kt)^{1/2}$. Obviously, $\beta_{pf} = 2\beta_s$ The field assisted thermal emission-limited current due to Poole-Frenkel effect is

$$J = A_{pf}(V/t) \exp[-\phi_o/kT] \exp[e\beta_{pf}V^{1/2}/kT] \qquad (1.13)$$

where $A_{pf}$ is a constant Such a conduction was observed by Vermilyea [25] and Simmons [26] assumed the presence of both

10
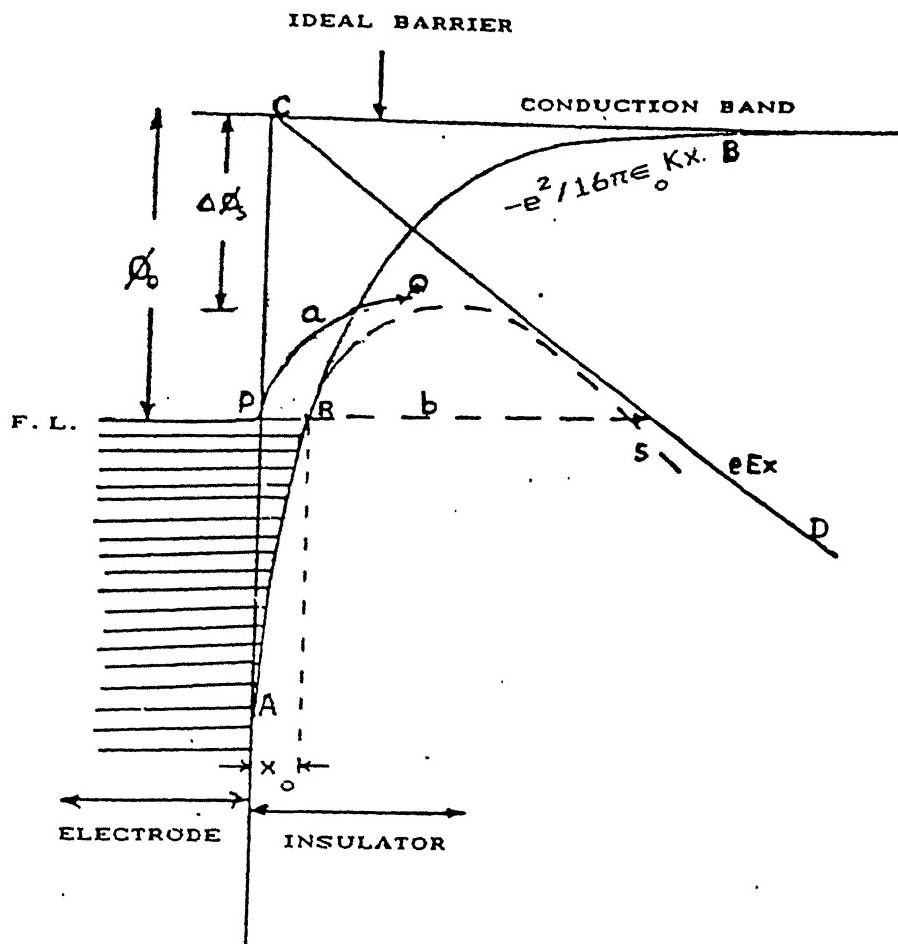
Fig. 1.5 Energy diagram of Schottky effect at a neutral contact under applied electric field.
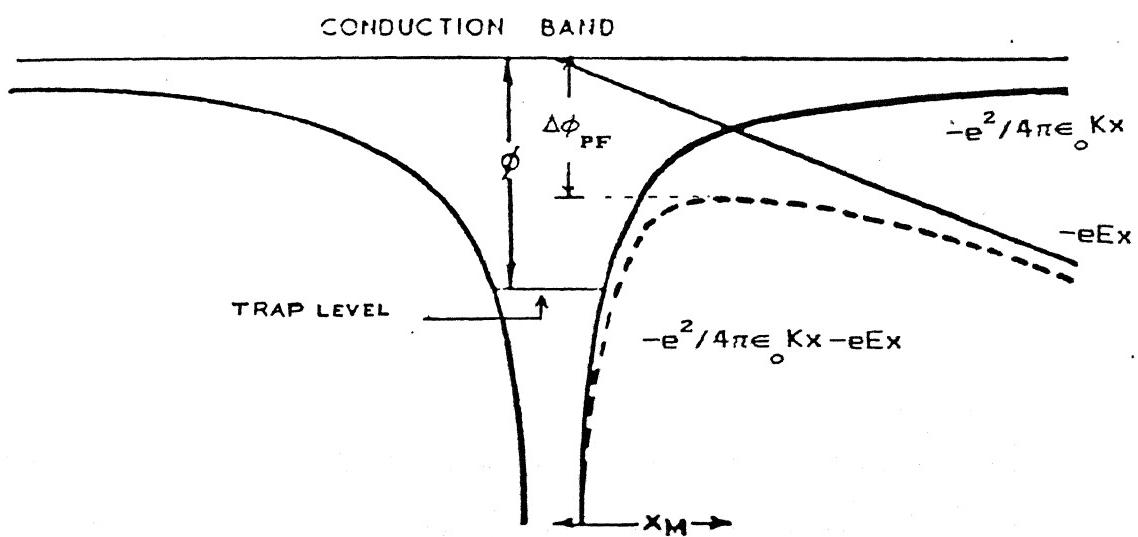
Fig.1.6 The lowering of the potential barrier for thermal excitation of trapped electrons into the conduction band of the insulator by an external electric field [25].

the traps and and the donors both in the insulator and modified Poole -Frenkel current contribution as

$$J = A_{pf}(V/t) \exp (\phi_o/kT) \exp (e_{pf}V^{1/2}/2kT) \qquad (1.14)$$

although The voltage dependence current density appearing in the exponential term is the same in equations (1.11),(1.13)and(1.14) yet, the difference is that while Schottky emission is electrode limited, process and Poole Frenkel effect is bulk limited process. Also, the electrode limited process can not continue indefinitely as the resistanceof contact decreases more rapidly than that of bulk with increase in voltages. Hence, at bias beyond a certain voltage value $V_t$(say, at which contact resistance falls to the bulk value), the current is essentially controlled by the bulk [11,26,27].

1.1.4 *Space charge limited (SCL) current:*

The electrons injected from the metal electrode through ohmic contact create space charge in the conduction band of insulator. This in turn, controls the electron injection thereafter. . The net current that results is termed as space charge limited ( SCL) current. Such a current may involve one or two carrier(s) with or without traps / recombination centres. Also, the traps can be shallow or deep in nature. For a trap free perfect insulator of thickness t, the space charge limited current $J_{scl}$determined by electron ejection and the applied field (V/t),is given by Mott and Gurney law [28]

$$J_{scl} = \frac{9}{8} \varepsilon_o K \mu \frac{V^2}{t^3} \qquad (1.15)$$

where K is dielectric constant of insulator and $\mu$, $\varepsilon$ are electron mobility and permittivity of free space and t is insulator

thickness. At low voltages , injected current density is less than the thermally generated free carrier $(n_o)$ and therefore the current obeys Ohm's law

$$J = en_o\mu(\frac{V}{t})$$ (1.16)

But, a transition occurs when the currents by equations(1.15) and (1.16) become equal, ie. at a voltage $V_{tr} = 8en_o t^2/9\varepsilon_o K$. The injected carriers are, however tapped within the insulator causing reduction in the overall space charge limited current[29]. The current-voltage characteristics can be devided[18] into four regions by considering the presence of shallow traps in the insulator [Fig1.7] . At low voltages the injected current density is less than thermally generated free carrier current density and Ohm's law is obeyed ,ie., region 1. At a voltage $V_{tr}$ transition occurs and current becomes space charge limited but is modified by the traps, ie, region 2. When all the traps are occupied, the current rises abruptly as in region 3. and reaches a value corresponding to a trap free insulator case ie., region 4 . The value of trap free limited voltage $V_{tfl}$ is given by

$$V_{tfl} = eN_t t/\varepsilon^2 K$$ (1.17)

where $N_t$ stands for the trap density. If the traps have distribution profile in terms of energy (ie . shallow and deep ). the space charge law is further modified such that [18]

$$J = \frac{9}{8} K\varepsilon_o\mu \frac{V}{t^2} (\frac{n_o e}{C}) \exp (CV/eNtK)$$ (1.18)

Where C is the capacitance of the insulator . If the cathode and anode are Ohmic for electrons and holes respectively , both type of carriers are injected into the insulator . The resultant

14
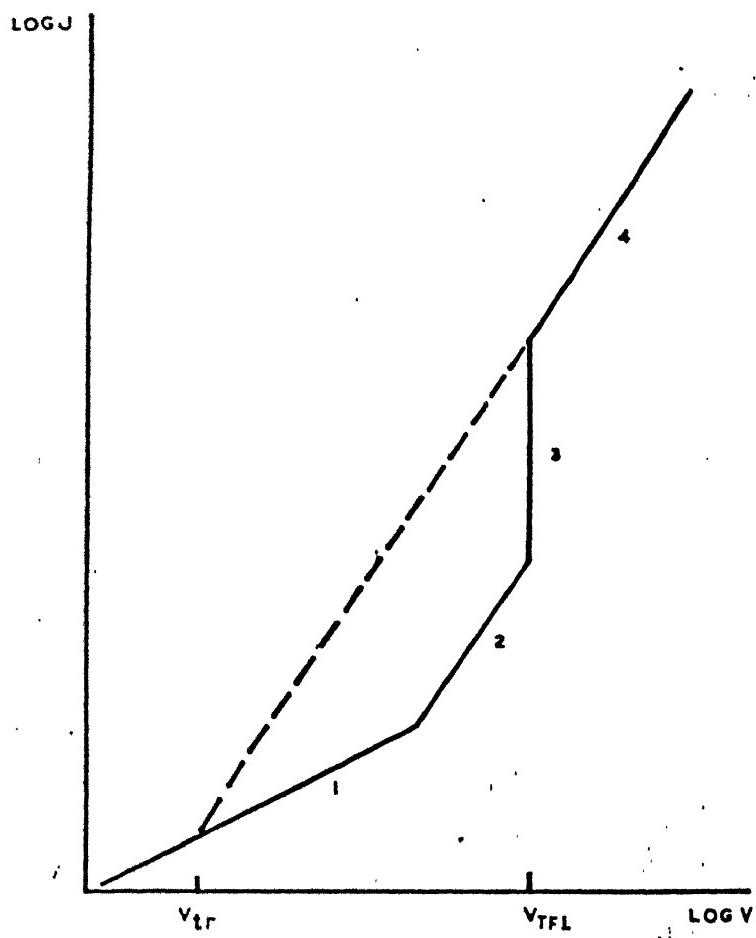
Fig. 1.7    One   carrier   space-charge   limited   current   -voltage characteristics for an insulator with a single trap level in four regions.

current becomes Ohmic or space charge limited depending on the relative magnitudes of the dielectric relaxation time $\tau$ and transition intervals ( $T_{re}$ and $T_{rh}$ ) for electrons and holes . When $\tau > T_{re}$ and $T_{rh}$ the current becomes space charge limited . At a critical voltage , Ohmic contact no longer exists and field emission occurs [30].

### 1.1.5 *Impurity conduction:*

According to Mott, insulator -metallic transition can occur for any array of atoms if the distance between them is decreased. The transition is sharp for an ordered array but smears out if randomness prevails. Obviously, as the concentration of impurities in an insulator increases and reaches a critical value,their average separation reduces such that the transition occurs. The activation energy $E_a$ for hopping decreases to zero and resistivity falls sharply . The insulator behaves like a conductor and it's resistivity becomes independent of temperature . Thus, the transition is essentially due to overlap of wave functions and occurs at a critical concentration (N'), such that

$$(36 \; \pi \; N')^{1/3} = 1/a_o \qquad (1.19)$$

Where $a_o$ is the Bohr radius of the impurity centre. The insulator has a very low density of thermally generated carriers at normal temperature. So, the conduction process involves mainly the electrons ofthe impurities  present despite their low mobilities. Actually, the electrons can either tunnel through or jump over the potential barrier from the occupied to an empty impurity centre. At low impurity concentration, the distance between the impurities is large and interaction is weak. The electrons are

16

then localized. Thus, electrons may hop from one site to another by emission or absorption of a phonon. An electric field produces an average gradient of energy and,in turn , causes a current flow in the field direction (towards lower field energy ). The resistivity $\rho(t)$ may be expressed as [18].

$$\ln \rho(t) = f(n) + E_a/kT \tag{1.20}$$

where $f(n)$ is the function of the carrier concentration and $E_a$ is the activation energy of the conduction mechanism. The resistivity is given by

$$\rho = \pi \hbar \ (3/\pi)^{1/3}/ \ n^{1/3} \ e^2 \ \alpha \tag{1.21}$$

where n free electron density and $\alpha$ is number 2 ratio of mean free path and the interatomic distance.

### 1.1.6 *Forming process and breakdown:*

With the application of increasing voltage, a stage is reached where MIM structures undergo a radial and permanent change. Here, the current rises several ordes in magnitude and followed by voltage controlled negative resistance (VCNR) characteristics [13,15]. This process is called forming and voltage of transition $V_f$ is termed as forming voltage. The occurrence of forming depends on nature of insulator, electrodes, impurity content and temperature [12,13,15,31-33].

The possible reasons of forming are (i) changes occurring in number of electrons due to Joule heating, (ii) setting up a of special semi-pemanent space charge distribution, and (iii) phase change and atomic rearrangement in the insulator[13]. The formed samples also show .VCNR, switching and memory effects[13]. after the forming, the conduction in the

insulator is due to electrons as well as ions. The forming voltage does not depend on the thickness of the insulator. However, the peak current obeys the relation [13].

$$I_{max} \propto 1/ (thickness)^3 \qquad (1.22)$$

Also, the forming voltage decrease with rise in temperature [16].There exists a maximum tolerable gas pressure $P_{inh}$ above which forming is inhibited. While an optimum gas pressure $P_o$ is required for forming to take place. $P_{inh}$ and $P_o$ vary widely from one insulating film to another depending upon the fabrication method, electrode metal,etc. [15]. The formed sample also shows the switching and memory effects. After forming, the conduction in the insulator is due to electrons and ions both when Breakdown occurs, the current rises very sharply and the insulator looses its properties and becomes a conductor. Such a change is radical and permanent in nature The breakdown is not a sudden process but appears with varying speed and in a range of electric field[13]. It occurs either due to avalanche or increase in temperature[3,4,35]. The conducting channels are created in the insulator at high electric fields,resulting in path for heavy current. Alternatively the conducting state is achieved due to thermal effects involving motion of defects and/or flaws in the insulator.

## 1.2 *Objective of the present work:*

Although numerous studies have been undertaken on MIM structures in the past, yet, their electrical properties are

still not fully understood [11,13,16-18,36-45]. Moreover, the effect of temperatures on the characteristics has not been investigated at all. An effort has therefore been made to study the current-density characteristics of Al-Al$_2$O$_3$-Al structures at various temperatures mainly to broaden our understanding of the conduction mechnism(s) involved. Moreover, aim has been to examine the effect of ageing on the J-V characteristics and study the temperature variation of capacitance.

The choice of Al$_2$O$_3$ lies in it's high stability, good insulating properties and reproducible characteristics. Also non porous, smooth homogeneous, defect free Al$_2$O$_3$ films can be prepared by thermal oxidation method [16,17,46].

## EXPERIMENTAL DETAILS AND PROCEDURES

### 2.1 *Substrate cleaning:*

We use glass slides of size 75mm x25mm x1mm as substrate for sample preparation. As these contain contaminants, grease, finger -prints, residue from manufacturing and packaging, we clean the slides with soap detergents in flowing water and allow them to dry. Subsequently, we rinsed these slides in acetone, subject to ultrasonic cleaning and keep them inside a clean bench for drying Finally, the cleaned glass slides are wiped with lint free tissue paper and transferred to a vacuum desiccator for storage.

### 2.2 *Bottom electrode preparation:*

Aluminum of 99.99% purity is deposited onto a glass subs- trate by thermal evaporation under vacuum using masks for yield- ing strips of length 75mm, width 0.8, 1.0, 1.25, 1.5mm and thick- ness ~ $0.25\mu m$. For this, aluminum charge is loaded in a pre- cleaned tungsten spiral mounted in the work chamber and evapora- ted by passing a low voltage and high amperage current after achieving a pressure of about $10^{-6}$torr. The glass slides are held at nearly 15cm from the source and, after coating with aluminium taken out and covered with silver paste (at locations for making electrical connections later), principally, to avoid oxidation there (Fig. 2.1).

### 2.3 *Oxide formation:*

Aluminium deposited glass slides are introduced in an electric oven and heated at 50, 100, 150 and $200^{\circ}C$ for 24h each in air. This process ensures oxidation of aluminum layer up to a certain depth which varies with the temperature used as discussed later in Section 3.1.

(a)

Bottom Aluminium film Electrode

1mm

1 mm

75 mm

25 mm

(d)

Top Aluminium Film electrode

75 mm

Al-Al$_2$O$_3$-Al structure

25 mm

Aluminium Film

Metallic connection

2500 Å

1 mm

75 mm

(b)

Al$_2$O$_3$ Formation

Aluminium Film

2500 Å

75 mm

Aluminium Film

75 mm

(c)
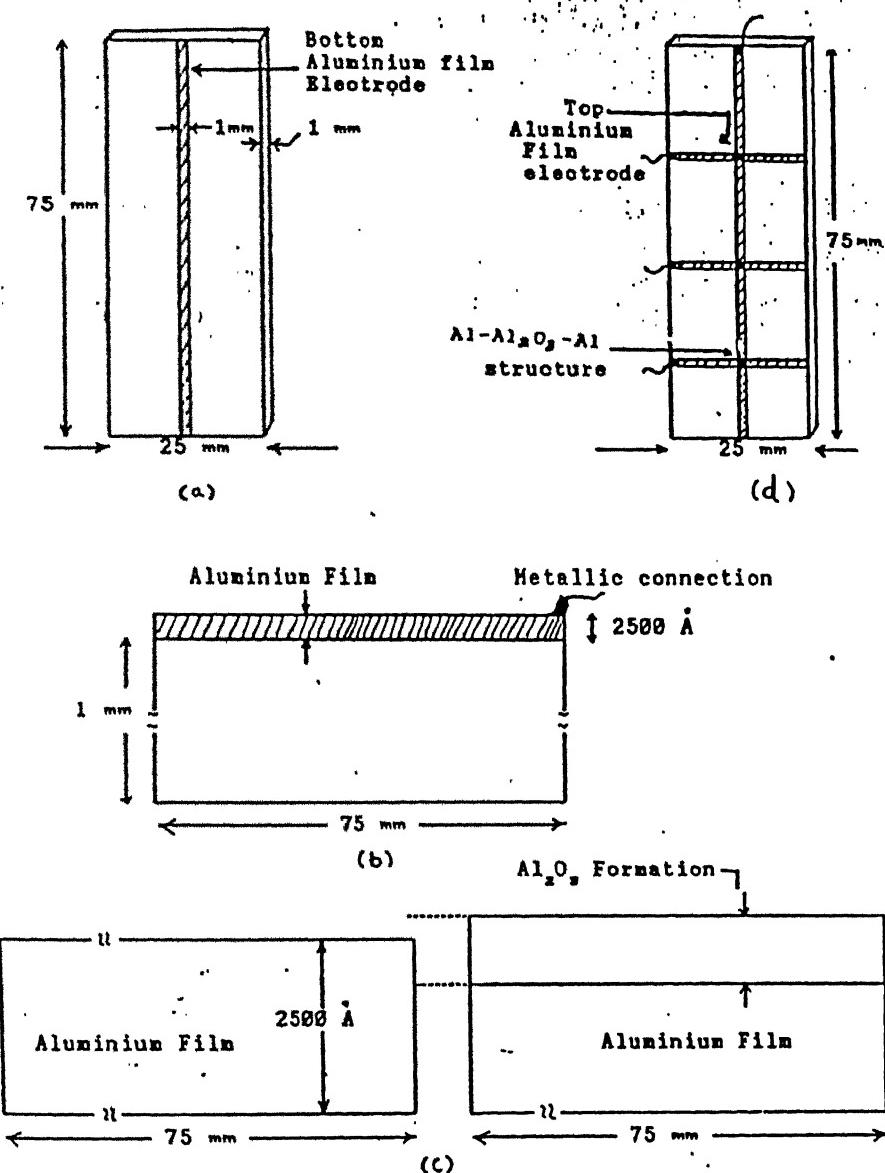
Fig 2.1 Different stages of preparation of Al-Al$_2$O$_3$-Al structures .

## 2.4 *Top electrode preparation:*

For this, aluminum is deposited as before (Section 2.2) onto the oxide through masks obliquely to the original strips (Fig.2.1 b). The electrical contacts are then made on top as well as bottom electrode with the copper wires using silver paste and allowed to dry in air for 1- 2h (Fig. 2.1d).

## 2.5 *Measurements:*

The junction areas of $Al-Al_2O_3-Al$ are determined accurately using an image analyzer Leitz ASM 68K and varioscan V16 video camera. Fig 2.2 shows schematically the experimental set-up used for I-V measurements. In this, we used a programmable voltage source KEITHLEY model 230 for bias application and an autoranging picoammeter KEITHLEY model 485 for measuring the current. These two are interfaced with a personal computer Zenith PC XT286 for automatic recording and storage of data. For measurements,voltage was raised in steps of 0.5V and the time duration between the two successive readings was kept at 3s. The circuit diagram for the current-voltage measurements is shown in Fig.2.3. The capacitance of $Al-Al_2O_3-Al$ structures are measured with a Hewlett-Packard LCR meter model HP 4276A at a frequency of 100Hz and a test voltage of 0.5V. For measurements above room temperature, we used a sample heater, specially constructed for the purpose, and control the temperature with a controller Indotherm-500. The temperature of the sample is detected independently by a thermocouple placed on the glass slide itself.
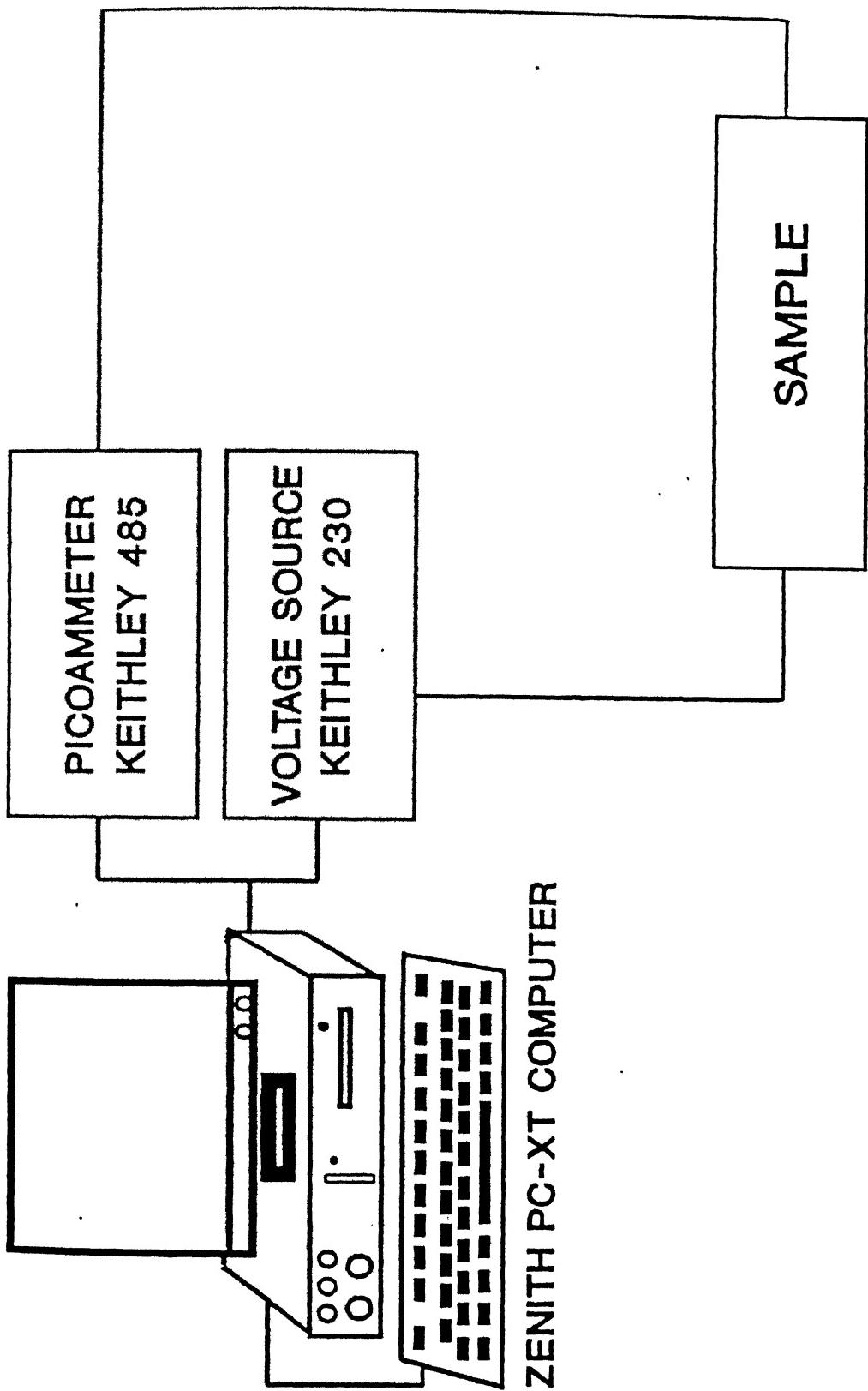
Fig. 2.2    Schematic diagram of the automated experimental set-up
used for current-density – voltage (J-V) measurements.
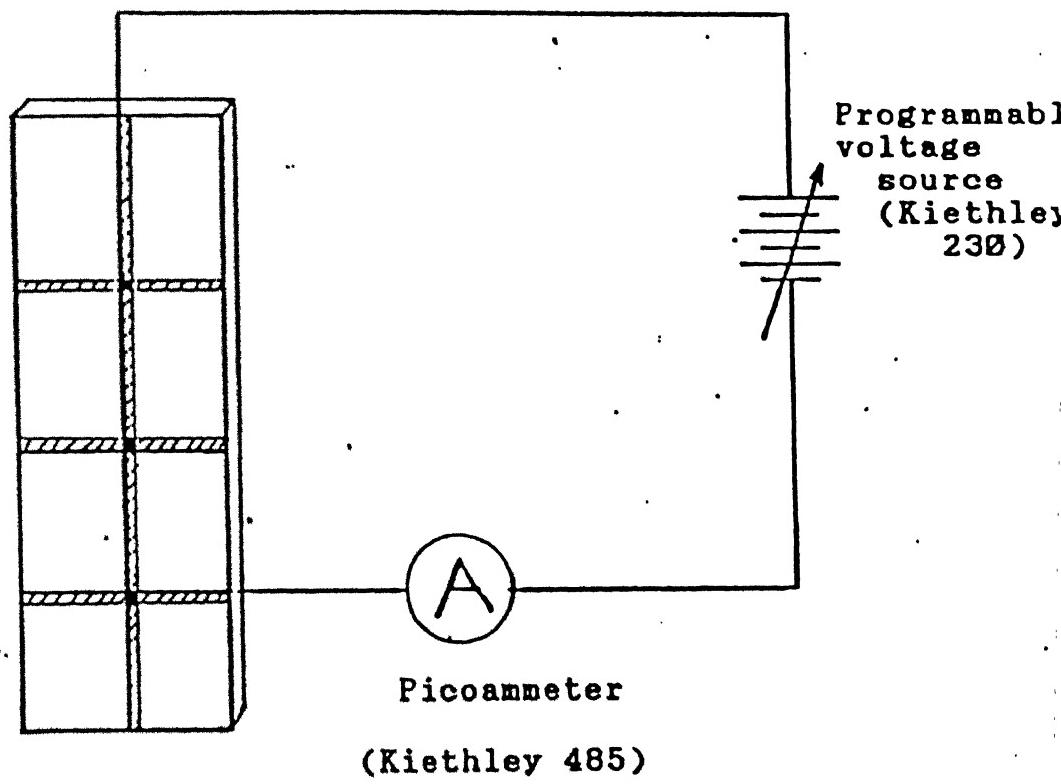
Fig. 2.3     Schematic     diagram     of     the     experimental     set-up     for
current     volage     (I-V)     measurements.

# CHAPTER - 3

## RESULTS AND DISCUSSION

### 3.1 *Oxide formation:*

Aluminum reacts with oxygen very slowly at room temperature. The initial oxide formation is very complex and involves process like physiosorption, chemisorption, absorption,etc.[47]. However, once initial oxidation occurs , further growth is sustained by movements of oxygen and/or aluminum atoms through the oxide for reaction at the oxide-aluminum and/or oxygen-oxide interface(s). Thus, the oxidation rate at this stage is governed by the kinetics of the reaction itself.

The protective ability of the oxide is quantified by the Pilling - Bedworth ratio ($\phi$)

$$\phi = \frac{\text{Molecular volume of oxide}}{\text{Atomic volume of metal}} = \frac{M_o d_m}{\eta^* M_m M_o d}$$

where $M_m$ is the atomic weight of the metal , $M_o$ is the molecular weight of the oxide , . $\eta^*$ is the number of metal atoms per molecule of the oxide and d is the density of the oxide. If $\phi$ is less than unity, the oxide fails to cover the entire metal surface and leads to a discontinues layer permitting easy passage to the oxygen. Thus, the amount of oxide formed depends only on the elapsed time at any given temperature. When $\phi$ is greater than unity, oxide occupies larger volume than the metal consumed and therefore protects the underlying metal efficiently The growth is then controlled by diffusion of oxygen and/or

metal atoms via the oxide layer. The value of $\phi$ for various $Al_2O_3$ modifications lies in the range 1.29-1.70 . Hence, the oxide is always protective in nature and also under the state of lateral compression. The latter may cause mechanical deformation, e.g., blistering occurs when adhesion is weak and cohesion is strong. On the other hand, shear cracking takes place when adhesion is strong and cohesion is weak. Aluminum oxide formed is amorphous and quite stable but transform to $\gamma$- $Al_2O_3$ above $500^{\circ}C$. Its work function is 5.4 ev. Further, $Al_2O_3$ has a large band gap (7eV) and exhibits ionic bonding and low current leakage characteristics. For thermal oxidation, aluminum films of thickness $\sim 2500\overset{\circ}{A}$ were heated in the air at 50, 100, 150, $200^{\circ}C$ for 12 and 24h each. This process leads to uniform and very stable amporphous oxide layers [16,17,46].

## 3.2 Current-voltage characteristics:

The J-V characteristics of MIM samples of various oxide thicknesses were recorded with bottom metal electrode as negative. Since the oxide films were invariably thin (i.e.,< $150\overset{\circ}{A}$ in thickness), measurements involve high electric field ( $\sim 10^{6}$ volt/cm) at potential of a few volts only. At such high fields, many conduction processes, viz., Ohmic, direct tunneling, Schottky emission, Poole-Frenkel effect, field emission may be operative in transporting the electric charges [13]. Obviously, the current may comprise of the contribution from all these processes, although the extent of each depends on thickness,

applied field and the nature of oxide. The typical current density-voltage characteristics of Al-Al$_2$O$_3$-Al structure, shown in Fig.3.1, may be divided into three distinct regions:(i) linear involving marginal increase in current with voltage and termed as Ohmic region, (ii) non-linear region exhibiting steep rise in current beyond a threshold voltage, and (iii) anomalous region at high voltages depicting high current followed by a negative resistance and fluctuations.

To identify the mechanism(s), it is usual practice to draw current density (J) – voltage (V) data in various ways(e.g.,Table 3.1). Accordingly, if ln (J) vs $V^{1/2}$ plot exhibits linearity in certain voltage range, conduction is determined by either the Schottky emission or Poole-Frenkel effect. To make distinction, in-depth analysis is required, in which, ln (J) vs $V^{1/2}$ and ln (J/V) vs $V^{1/2}$ plots are viewed together. If both of these plots show straight lines in the same voltage range, Poole-Frenkel effect is said to be applicable. On the other hand, if linear region prevails only in ln (J) vs $V^{1/2}$ plot, the operation of Schottky emission is indicated. Also, the presence of a definite minimum in the ln (J/V$^2$) vs 1/V plot is taken as a criterion for the existence of Schottky emission. Figures 3.2-3.6 show the J-V, lnJ-lnV, lnJ-$V^{1/2}$, ln(J/V$^2$)-1/V and ln(J/V)-$V^{1/2}$ plots at 25,40, and 60$^o$C. As expected, initially, the current varies linearly with voltage (i.e., exhibits Ohmi c nature). As temperature rises , the Ohmic region shrinks. Also, the slope (dI/dV) increases with temperature and amounts to decrease in the resistance of the Al$_2$O$_3$ and/or easy passage to carriers. Table
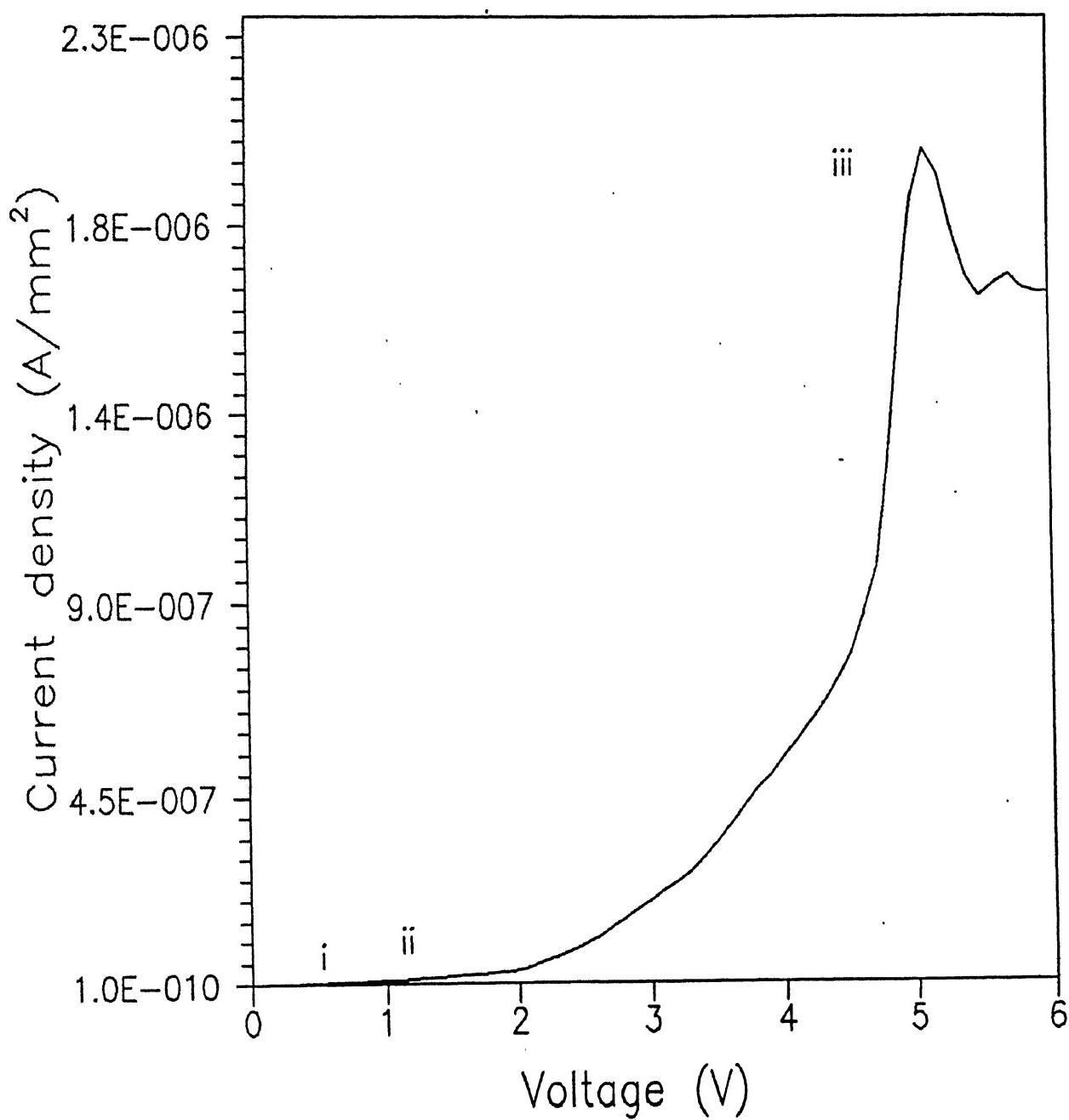
Fig. 3.1    Typical schematic  diagram of  current density-voltage
           (J-V) characteristics of $Al-Al_2O_3-Al$ structure showing
           three distinct regions.

Table 3.2 Characteristics of various conduction processes operating in thin insulating films.

| Conduction type | Plot(s) | Nature | Remark(s) |
|---|---|---|---|
| Ohmic | J vs V | Linear | Ohm's law $J \propto V$ |
| Space-charge limited | J vs V<br>ln(J) vs ln(V) | Non-linear<br>Linear with<br>slope=2<br>slope=3 | Child's law $J \propto V^2$<br>Cube law $J \propto V^3$ |
| Tunneling | $\ln(J/V^2)$ vs 1/V | Straight line with negative slope | Fowler-Nordhiem equation,<br>$J=J_o \{2.2(eV)^2/(4\phi_o)\}$<br>$\exp[-2A'\phi_*^{3/2}/(2.96eV)]$ |
| Schottky emission | ln(J) vs √V | Straight line with positive slope | Richardson-Schottky equation,<br>$J=A^* T^2 \exp(-\phi_o/kT)\exp(e\beta_s V^{1/2}/kT)$<br>slope gives field lowering coefficient $\beta_s$ |
|  | $\ln(J/V^2)$ vs 1/V | Curve with a definite minimum | Modified Schottky equation<br>$\ln(J/V^2) = B + B'\sqrt{V} + 2\ln(1/V)$<br>B and B' are constants |
| Pool-Frankel effect | ln(J) vs √V | Straight line | slope gives field lowering coefficient $\beta_{PF}$ |
|  | ln(J/V) vs √V | Straight line | Pool-Frankel current equation<br>$J = A_{PF}(V/t)\exp(-\phi_o/kT)$<br>$\exp(e\beta_{PF} V^{1/2}/kT)$<br>slope gives field lowering coefficient $\beta_{PF}$ |
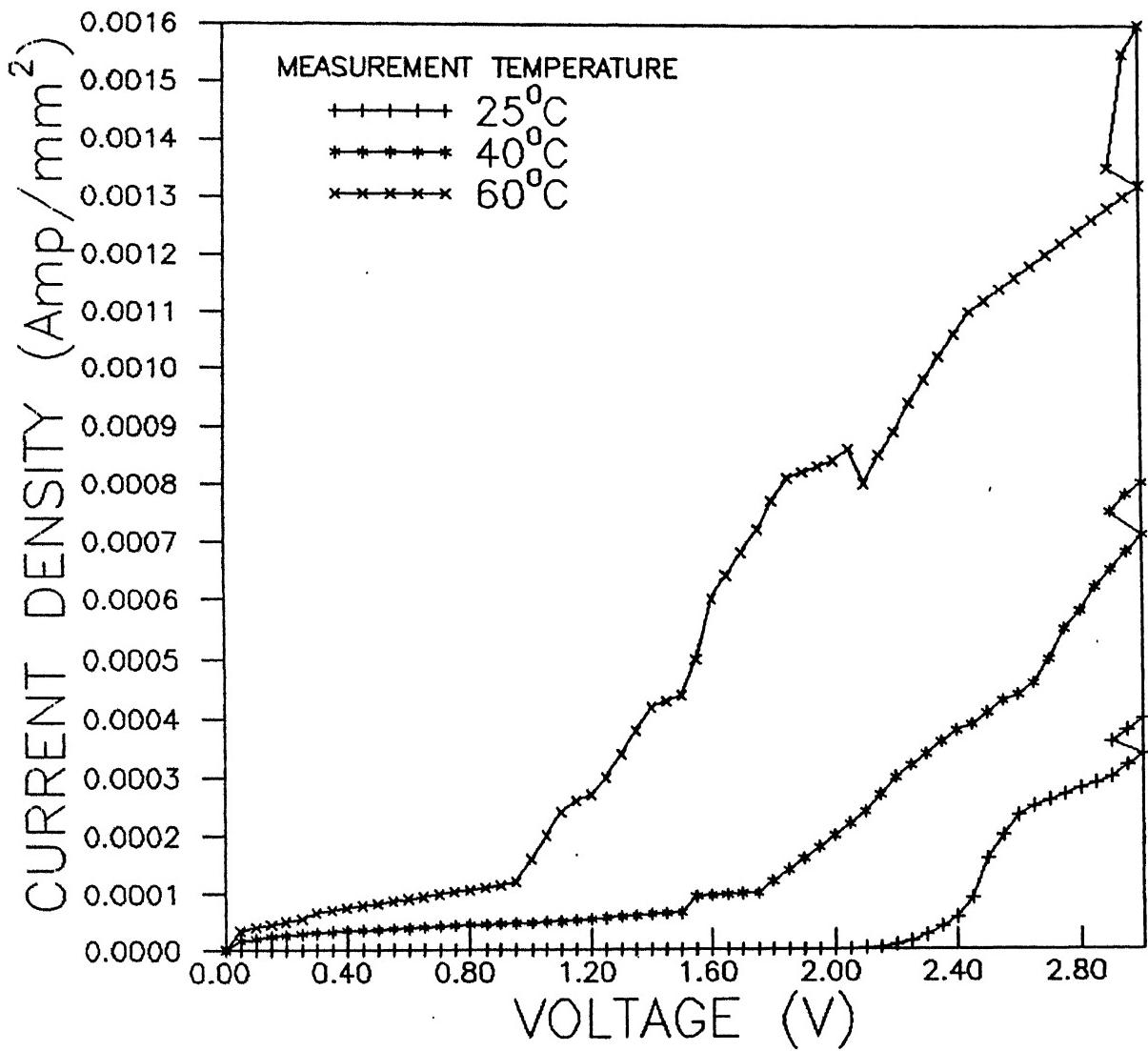
Fig. 3.2    Current density-voltage (J-V) plots   for $Al-Al_2O_3-Al$
structures with thermally grown oxides at various
temperature.
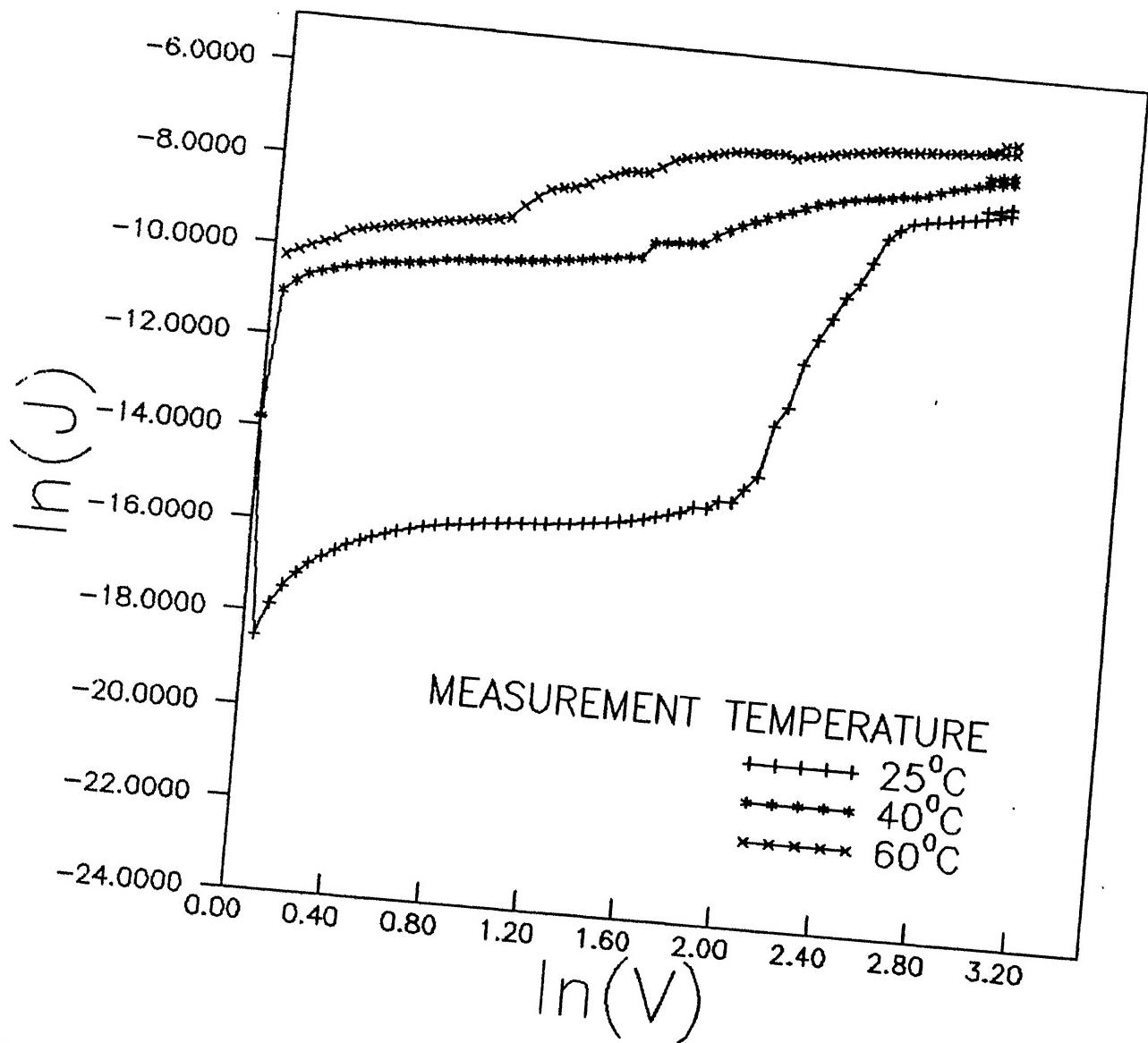
Fig 3.3    Logarthmic plots of the current density versus applied voltage for Al-Al$_2$O$_3$-Al structures at various temperature.
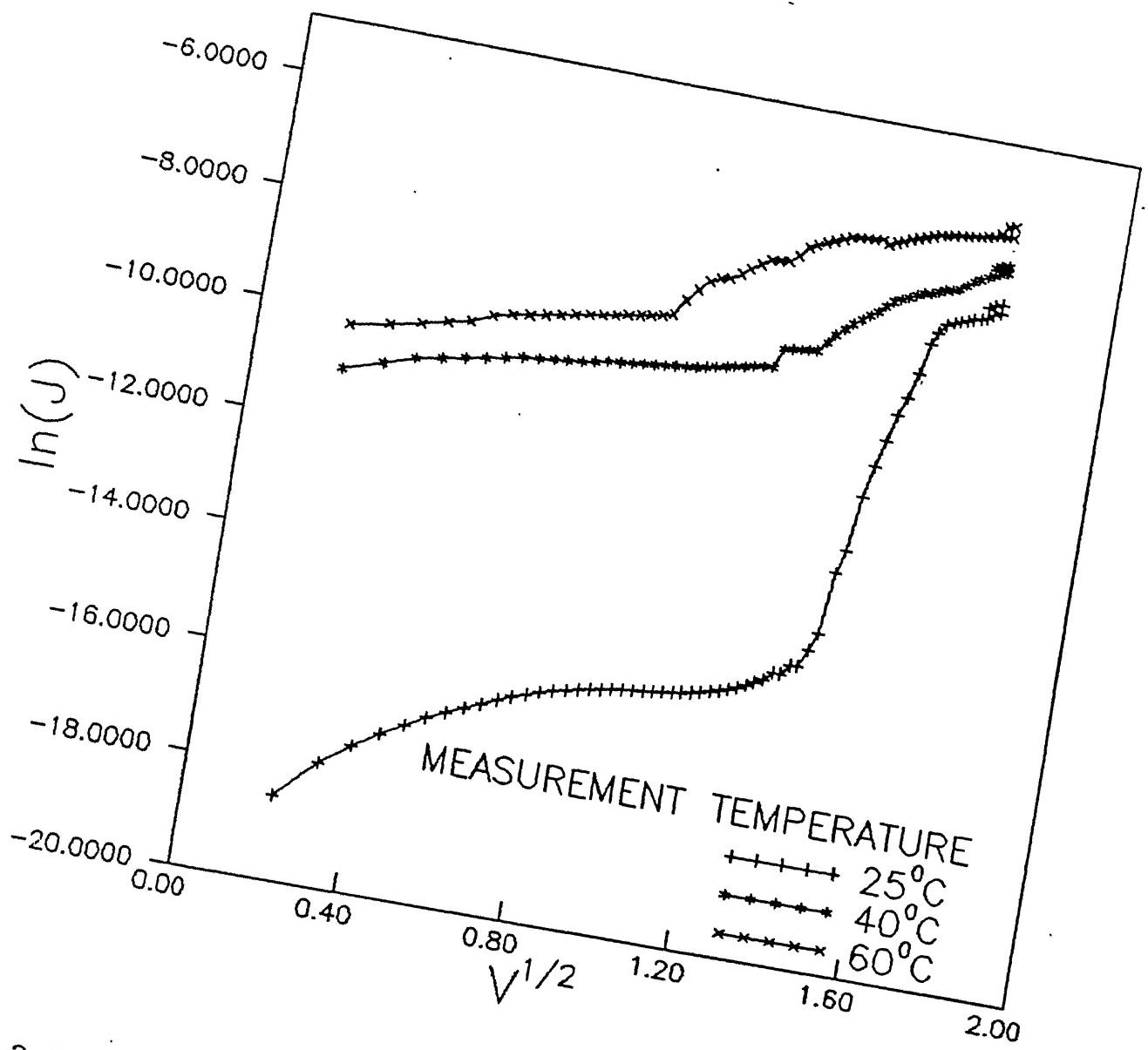
Fig.3.4   Ln (J) versus $V^{1/2}$ plots of Al-Al$_2$O$_3$-Al structures

32
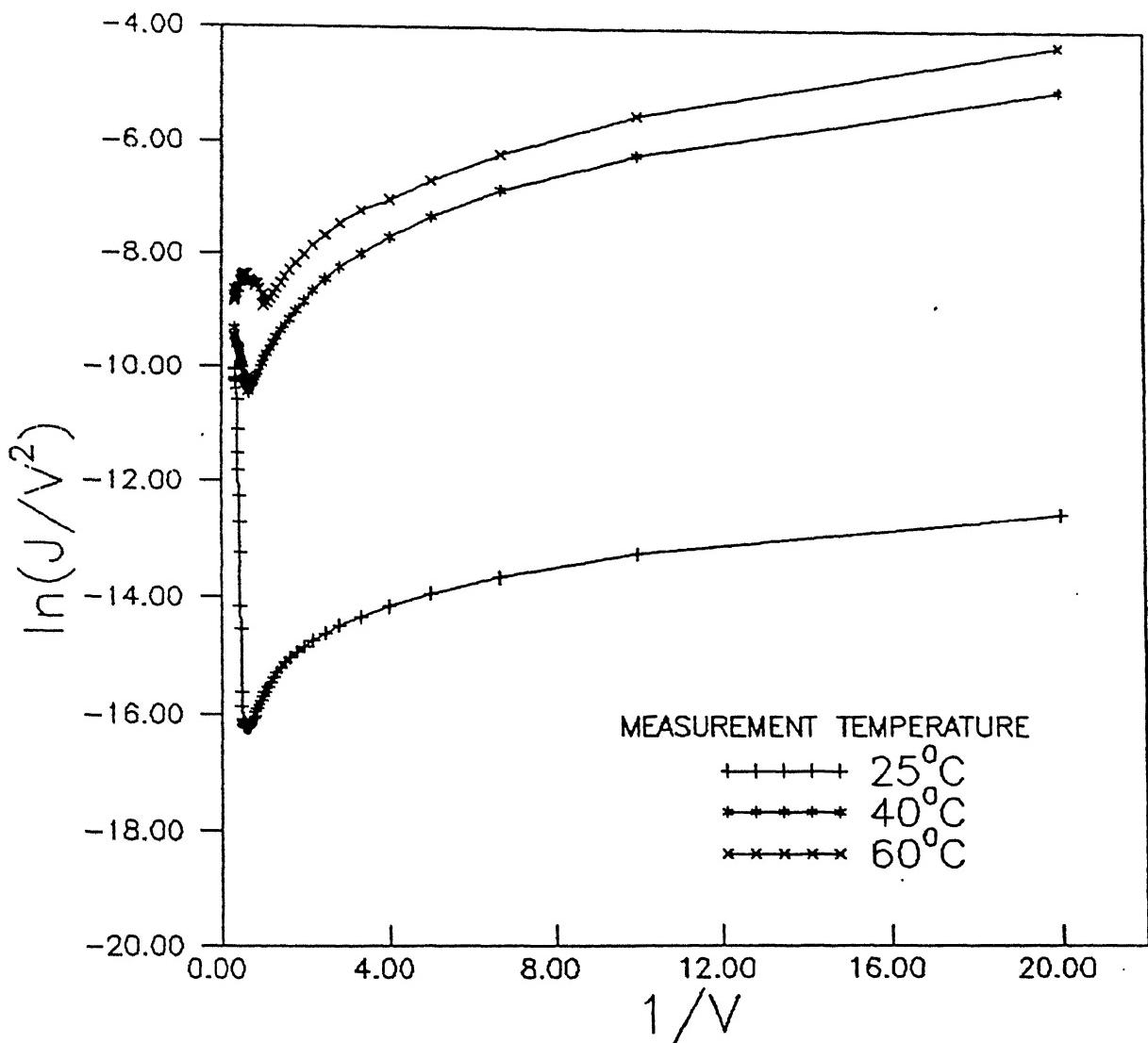
Fig.3.5    Ln $(J/V^2)$ versus $V^{-1}$ for $Al-Al_2O_3-Al$ structures
at various temperatures.
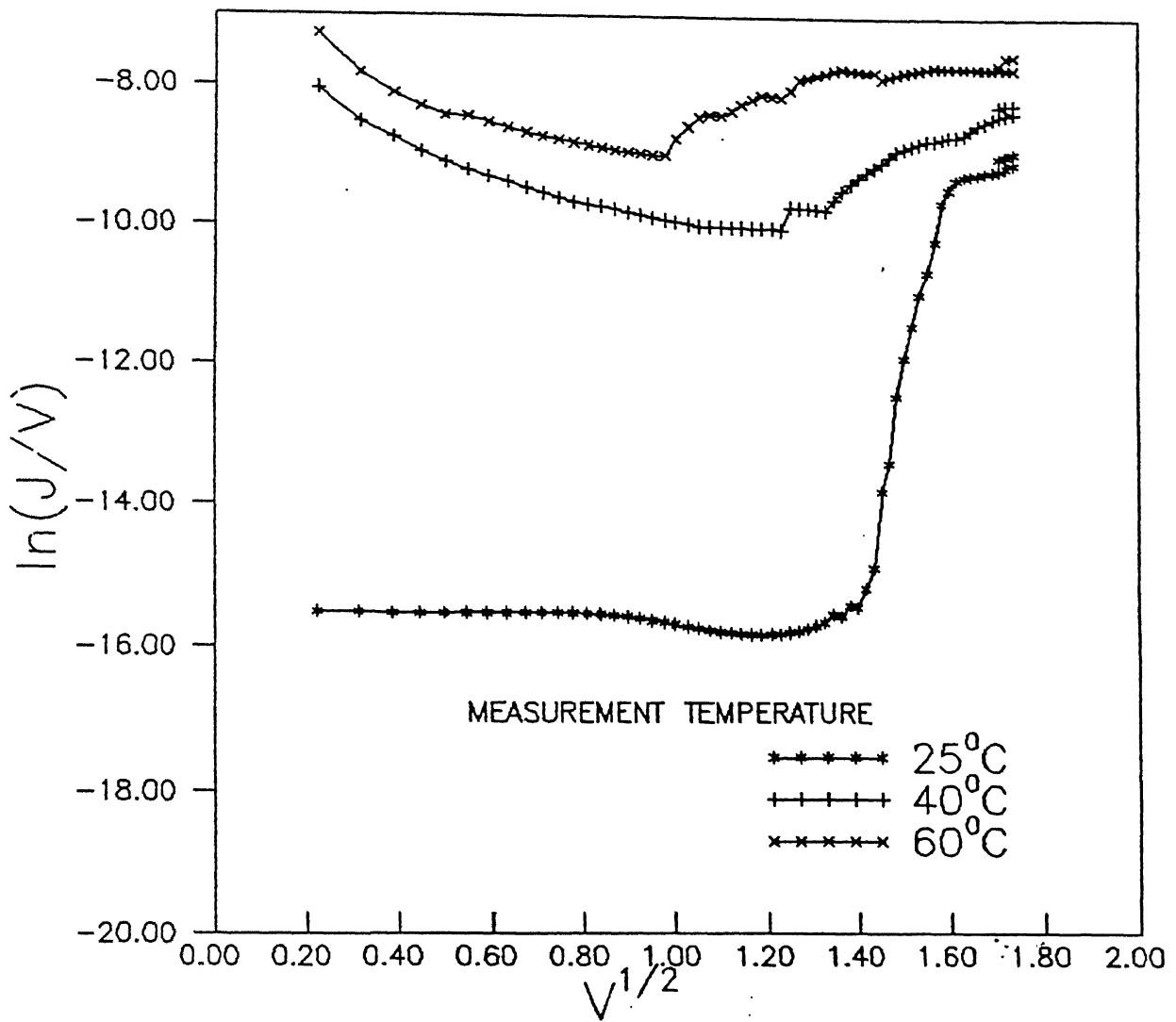
Fig.3.6 Plots of ln (J/ V) versus $V^{1/2}$ for Al-Al$_2$O$_3$-Al structures at various temperatures.

3.2 summaries the analysis of J-V data based on the above plots. Accordingly, Ohmic, Schottky emission and field assisted tunneling are clearly operating in different voltage ranges for all the $Al-Al_2O_3-Al$ structures at 25, 40, 60$^o$C. We also noticed t hat Schottky emission and field assisted tunneling get initiated progressively at lower voltages with increase in temperature. The intercepts at the ordinate of the extrapolated straight lines corresponding to the Schottky emission in the ln(J) verses $V^{1/2}$ plots are taken to evaluate the values of barrier height as per equation (1.11) [24]. The values obtained are given in Table 3.3 and found to be in good agreement with those reported at room temperature by Emptage and Tantraporn [23], Antula [48], Madhukar [17]; their values bei n g 0.7eV, 0.74eV and 0.727 -0.775 eV, respectively. As we increase the temperature, the barrier height $(\phi_o)$ decreases slightly. That means the conduction process becomes somewhat easier at higher temperatures. Similarly,barrier lowering coefficient determind from the J-V data using slopes of ln (J) vs $V^{1/2}$ plots in the linear region is also given in Table 3.3, Its increase with temperature amounts to overall decrease of the barrier height - consistent with the above observation.


3.3 *Variation of capacitance with temperature:*


To examine the nature of $Al-Al_2O_3-Al$ structure further, capacitance was mesured as a function of temperature. Fig (3.7) shows capacitance verses temperature plot of samples containing thermally grown $Al_2O_3$ at 50, 100, 150, and 200$^o$C in laboratory

Table 3.2 Voltage ranges of different conduction processes at various temperatures of Al-Al2O3-Al structures having oxide grown at 100°C for 24 h in air :

| Measurement Temperature (°C) | Ohmic Range (V) | Schottkey range (V) | Field assisted tunneling (V) |
|---|---|---|---|
| Room temperature (25) | < 0.60 | 0.8 - 1.5 | > 1.85 |
| 40 | < 0.45 | 0.45 - 1.45 | > 1.75 |
| 60 | < 0.25 | 0.25 - 1.00 | > 1.50 |

Table 3.3 Parameters obtained for Schottky emission at various remperatures for Al-Al2O3-Al structures having oxide grown thermally at 100°C

| Measurement Temperature (°C) | Schottky barrier height $-\phi_o$(eV) | Schottky barrier lowering coeff. ($\beta s$) |
|---|---|---|
| Room Temperature 25 | 0.704 | 0.055 |
| 40 | 0.700 | 0.058 |
| 60 | 0.660 | 0.060 |
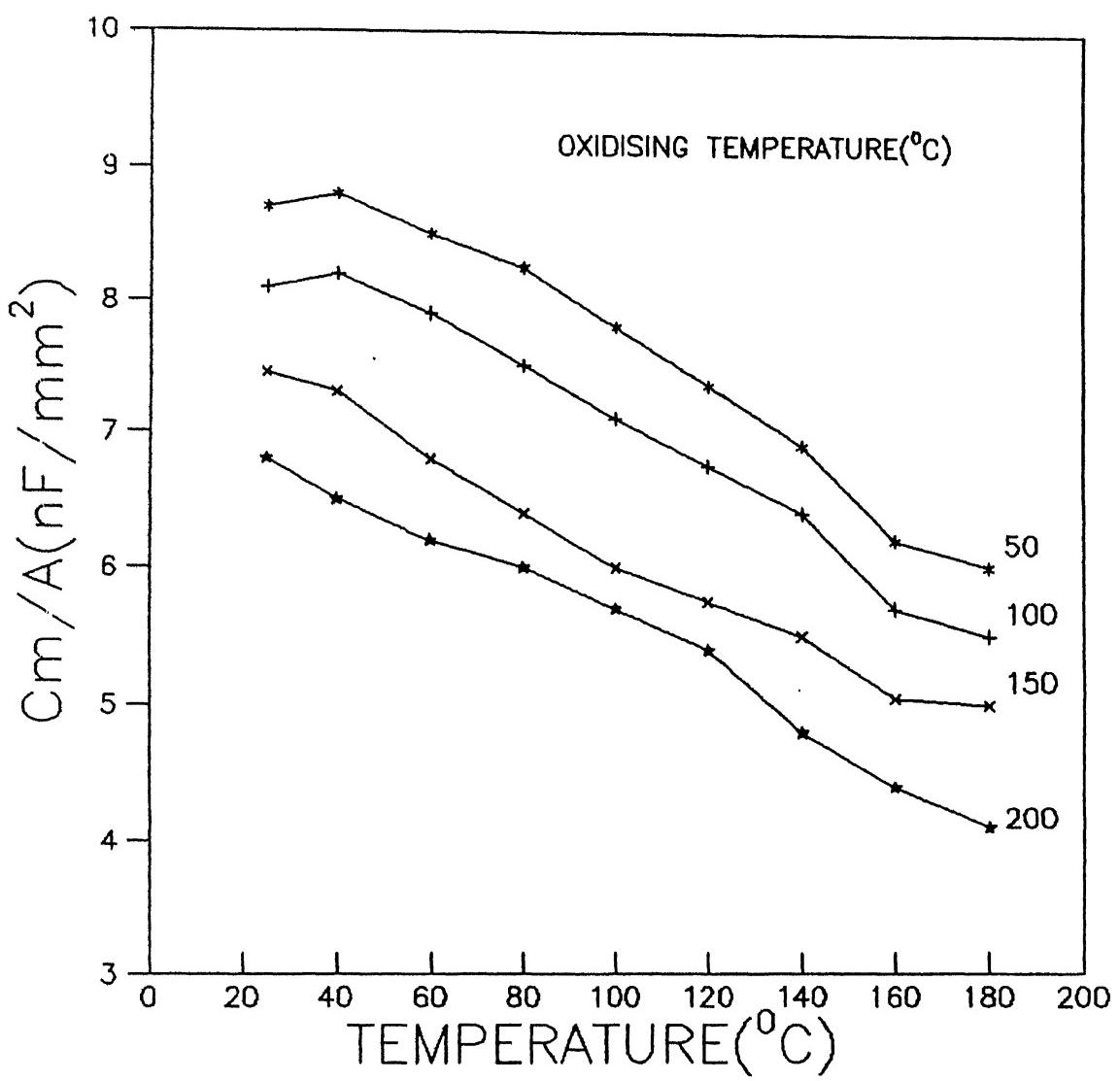
Fig. 3.7    Temperature variation of capacitance per unit area of

Al-Al₂O₃-Al junction prepared with oxide grown at

50,100,150 and 200°C.

air. Clearly, capacitance either decreases or first increases marginally and then decreases continuously. Also, the capacitance values are higher for those films which are grown at lower oxidizing temperature, i.e., where thickness is smaller. As the oxidizing temperature increases the oxide thickness also increases. It leads to reduction in the capacitance.

According to Hebard, Ajuria and Eick [49], the measured capacitance ($C_m$) of M-I-M structure of area 'A' and insulating thickness 't' can be considered as a series combination of interfacial and geometric components ($C_i$) and ($C_b$), such that

$$\frac{A}{C_m} = \frac{A}{C_i} + \frac{t}{\varepsilon_o K} \tag{3.1}$$

where K is the dielectric constant and $\varepsilon_o$ is the permittivity of the free space. The geometric or bulk capacitance is given by $C_b = K\varepsilon_o A/t$. Thus, $A/C_m$ vs oxide thickness (t) plot should yield a straight line having an intercept at the ordinate to give the interfacial capacitance ($C_i$). For this purpose, they determined the oxide thickness by optical interference method [50] and found the values of interfacial capacitance as 1.62 $\mu F$ /cm$^2$ for Al-Al$_2$O$_3$-Al structure having oxide thickness less than 360Å. Here, an inherent assumption was that the interfacial capacitance ($C_i$) is proportional to area only and independent of oxide thickness. Also, the dielectric constant (K) is believed to remain unaffected by the changes in the oxide thickness. On the other hand, bulk capacitance decreases with increase in oxide thickness. Since the bulk and interfacial capacitance lie in series, the measured data actually correspond to the smaller value of the two components. A

simple calculation reveals that the interfacial capacitance become more comparable for 50Å thick $Al_2O_3$ with K =9.03. As oxide thickness increases, $C_b$ decreases and on attaining 1/10 or 1/100 of the interfacial capacitance $C_i$, measured values should be 90% or just the bulk capacitance; the corresponding oxide thickness being 500Å or 5000Å. For relatively thin oxides , interfacial capacitance is very large. As the thickness of $Al_2O_3$ in the present case is expected to be less than 200Å, the interfacial capacitance contribution is likely to be quite significant [49, 51, 52]. Fig.3.8 shows $A/C_m$ vs oxidation temperature (T) plots of Al-Al2O3-Al structures at 25, 60, 100, 140 and 180°C. Accordingly, $A/C_m$ depicts a greater value with rise in the oxidation temperature. Also. $A/C_m$ for any particular sample (i.e, having $Al_2O_3$ grown at 50, 100, 150 or 200°C) increases with the measurement temperature. Fig (3.9) shows $A/C_m$ as a function of oxide thickness ( determined using eqn. 3.1 from the room temperature capacitance data using $C_i$ = 1.62 $\mu F/cm^2$ and K = 9.03) of various Al-$Al_2O_3$-Al structures. These clearly reveal that $A/C_m$ increases with oxide thickness at every measurement temperature, presumably due to bulk contribution. Also, the intercepts at the ordinate corresponding to zero oxide thickness assume progressively a larger value. This means that the interfacial contribution to $A/C_m$ is increasing with temperature. In other words, the interfacial capacitance is decreasing with rise in temperature. It appears that the charges present at the interface are getting annealed out. These results also suggest that with rise in temperature $C_i$ is approaching to a constant value progressively as
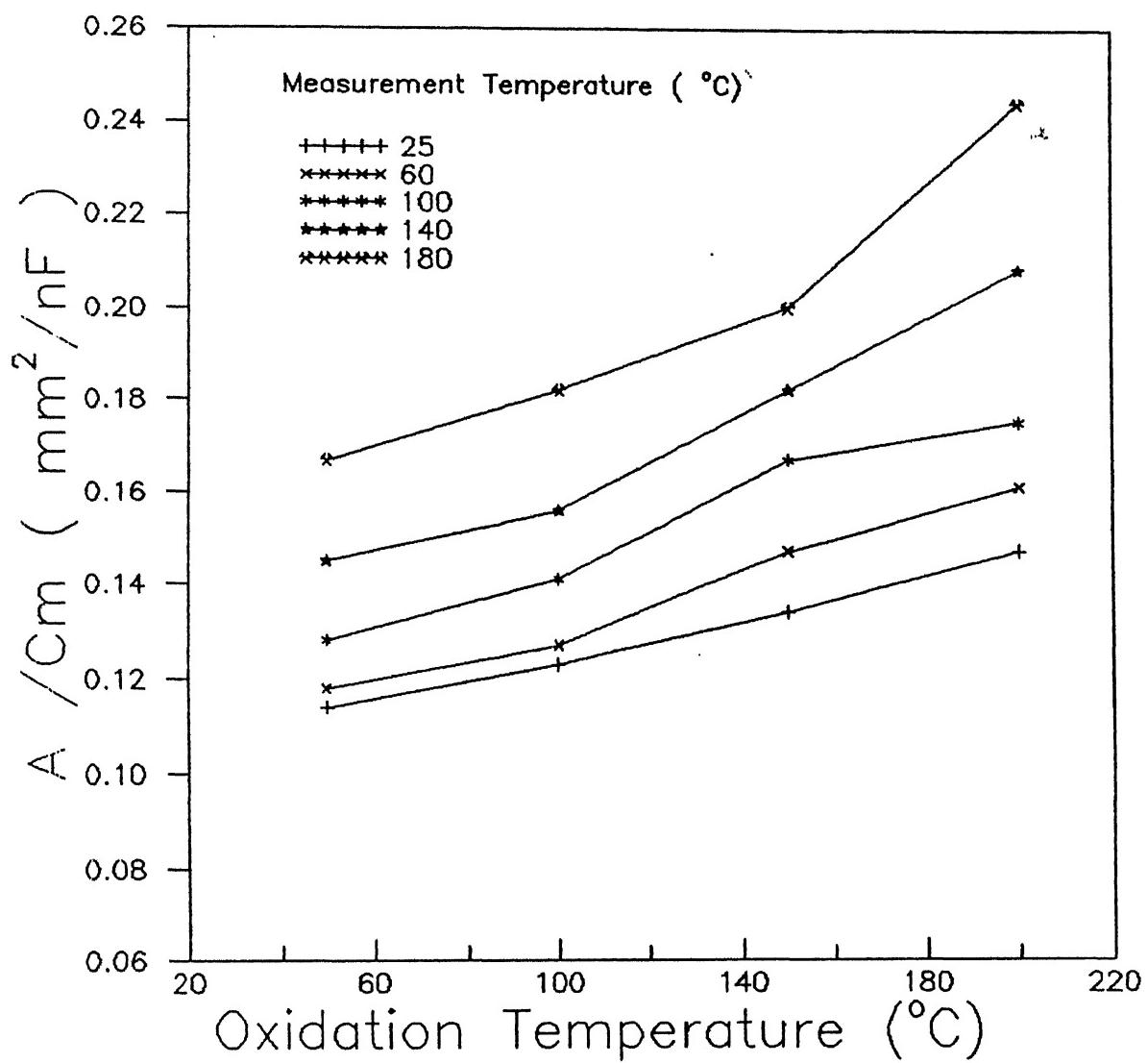
Fig. 3.8    Inverse measured capacitance (A/Cm) as a function of oxidation temperatures.
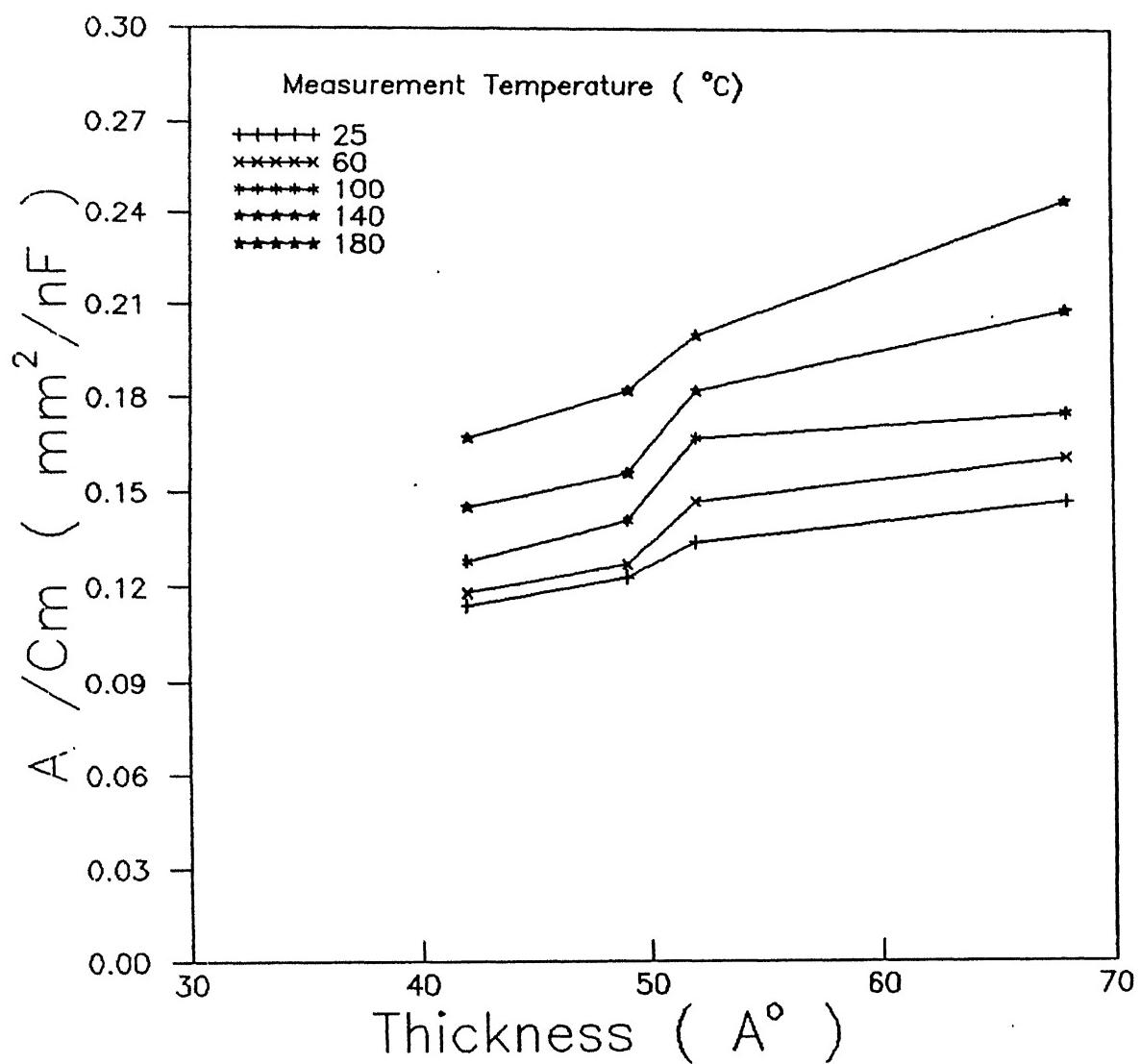
Fig. 3.9    Inverse measured capacitance (A/Cm) as function of oxide thickness (t) for Al-Al2O3-Al structures at various temperature.

the increase in the intercept value is decreasing continuously. Although, it is difficult to fit $A/C_m$ versus oxide thickness data with straight line exactly at every temperature, still one notices the trend of increase in the slope. One may then infer that even bulk contribution to the inverse capacitance is increasing with temperature. This could happen if oxide thickness is increasing or the value of dielectric constant is decreasing. The former is not likely because of protection of the oxide from both faces. The later is perhaps possible and may be attributed to the neutralization of charges present in the bulk $Al_2O_3$ with increase in temperature. Alternatively, since the interfacial capacitance is continuously decreasing with temperature, its separation from the measured data is not at all possible. This inhibits determination of the nature of real changes in bulk value of the capacitance. In all probability, the decrease in measured capacitance is mainly due to change in the interfacial effects. The temperature coefficient of capacitance $(C_m)$ and dielectric constant K are defined as [45]

$$\gamma_c = 1/C_m \ (dC_m/ \ dT) \tag{3.2}$$

$$\gamma_p = 1/K \ (dK \ / \ dT) \tag{3.3}$$

also $\gamma_p$ and $\gamma_c$ are related, such that

$$\gamma_c = \gamma_p + \alpha \tag{3.4}$$

where $\alpha = 1/3V \ (dV/dT)_p$ is linear expansion coefficient of the dielectric. The dielectric constant K depends on the contribution of $\varepsilon_e$, $\varepsilon_n$ and $\varepsilon_d$ arising due to electronic polarizability , ionic polarizability caused by vibration of the nuclei and deformation of ions, respectively, which themselves change with temperature

[45]. It is convenient to examine them together by involving Clausius and Mosotti equation, which relates dielectric constant to the polarizability ($\alpha_m$) and volume V as

$$(K-1)/(K+2) = \alpha_m/(2\varepsilon_0 V) \qquad (3.5)$$

By differentiating with respect to temperature T and using equations (3.3 and 3.4), one obtains

$$\gamma_c = \frac{(K-1)(K+2)}{\varepsilon} \left[ \frac{1}{3\alpha_m} \left(\frac{d\alpha_m}{dT}\right)_p - \alpha \right] + \alpha \qquad (3.6)$$

Interestingly, the values of $\gamma_c$ for a large number of materials lie on the curve (see Fig. 3.10) described by equation (3.6). Accordingly, $Al_2O_3$ lies near the peak, where ionic and electronic polarizability are comparable [45]. We also see that beyond the peak , $\gamma_c$ decreases linearly with the increase of dielectric constant. In this region, the contributions of ionic polarizability and deformation of ions dominate. Since $\gamma_c$ is positive for $Al_2O_3$ (Fig.3.10), one expects the measured capacitance to increase with rise in temperature. The present data appear to be in contradiction with this description as the capacitance is found to decrease with rise in temperature. As mentioned earlier, the measured capacitance, in fact, contain interfacial contribution which itself varies with temperature and hence its separation is not straight forward so as to estimate the change in the bulk contribution. The rise in bulk capacitance with temperature is perhaps getting masked with the interfacial contribution.

3.4 *Breakdown and ageing phenomenon:*

As we know, all insulators behave like intrinsic semiconduc-
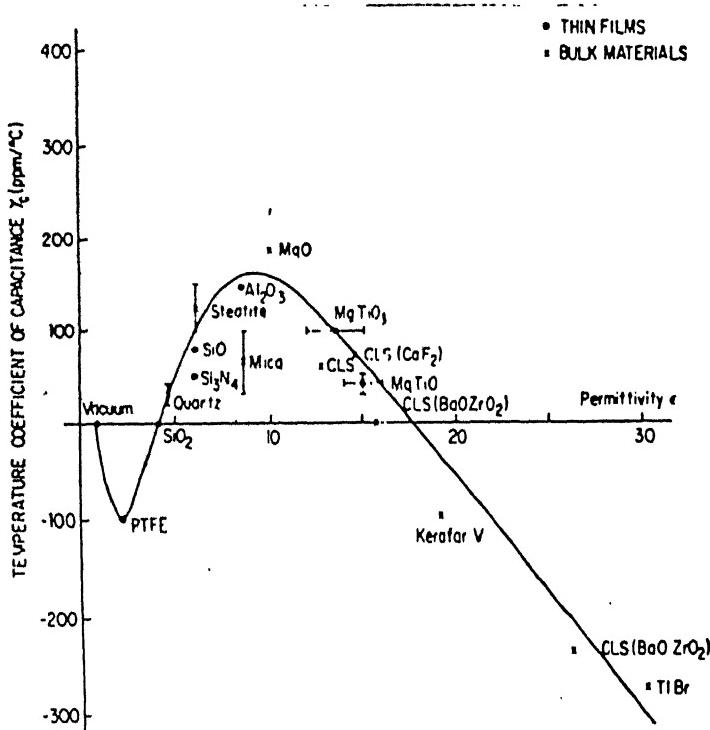
Fig. 3.10    Temperature coefficient of capacitance $\gamma$c vs. dielectric coefficient for materials with low losses[45]

tors. Above absolute zero, the conduction through them can therefore take place by excitation of electrons. The presence of structural defects and impurities may, however, facilitates this process and give rise to ionic current. On application of an increasing electric field, a stage reaches when large current flows through the insulator (or dielectric) and breakdown is said to occur. The insulator then attains a conducting state and the voltage across that falls to a near zero value. The breakdown may be caused by applying a threshold voltage (or electric field) across or by raising the temperature to a sufficiently high value [34,35,41-43,53]. Also, the current flow heats up the insulator and results in a permanent deformation. The process usually starts at inhomogeneities and propagates rapidly in other directions within a few micro seconds. The inhomogenities present display dark dots in electron microscopic images [54]. Thermal breakdown is produced when the heat generated by the current is faster than the dielectric can dissipate. Since the thermal conductivity of insulator is invariably low, the heat causes the local rise in temperature or even melting sometimes. This generates more carriers and increases their mobility, leading thereby to breakdown. As a consequence, various destructive effects may take place, e.g., creation of channels of molten material and/or jagged holes.

Avalanche breakdown refers to large and continuous increase in the number of electrons with the applied field reaching to a critical value. Usually a field ~ $10^6$ volt/cm is required to cause the avalanche breakdown irrespective of prevailing temperature. It
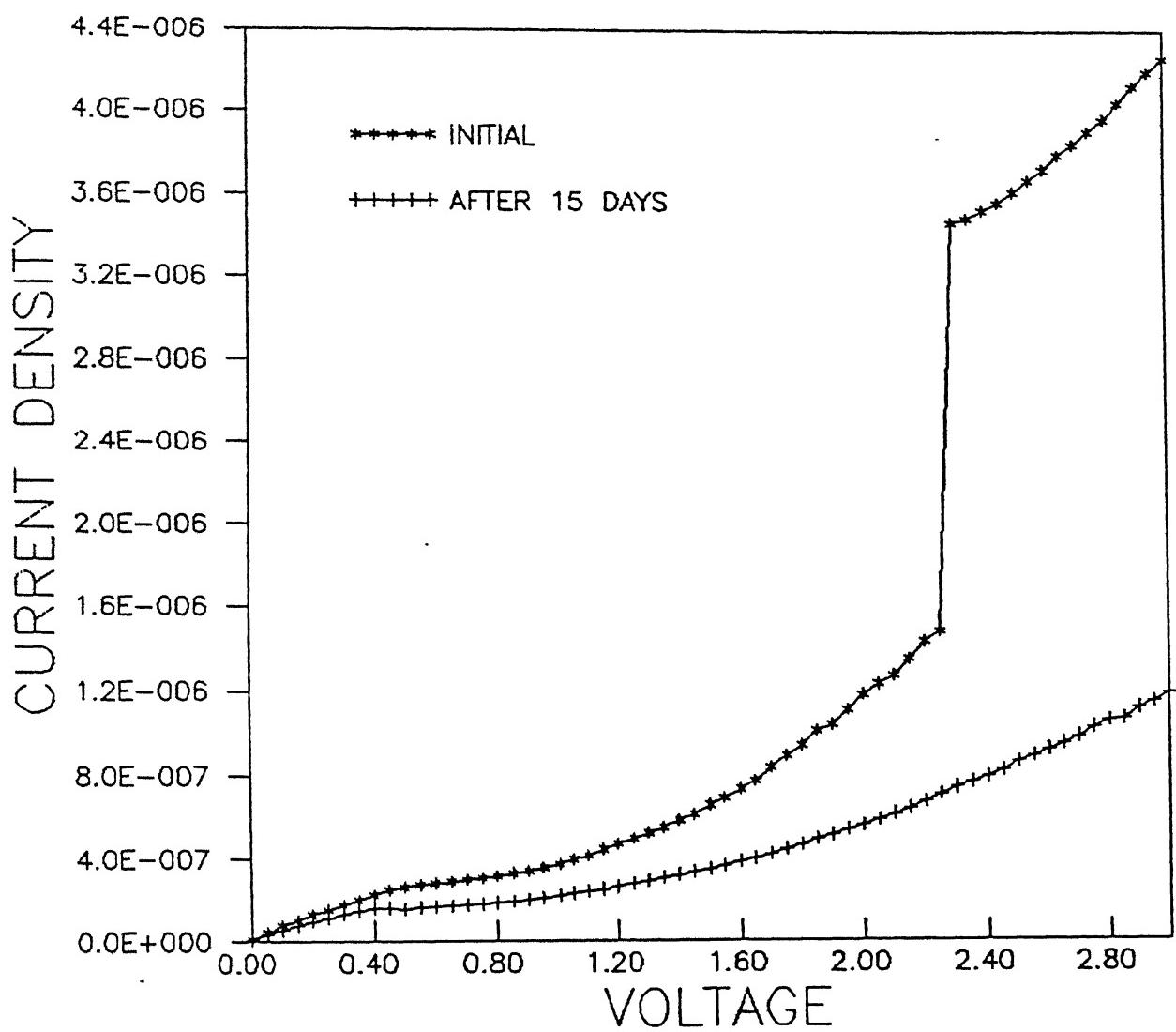
Fig.3.11 The J-V characteristics of a sample having oxide grown at $100^{o}C$ and junction area of $0.70mm^{2}$ as such and after 15 days of ageing.
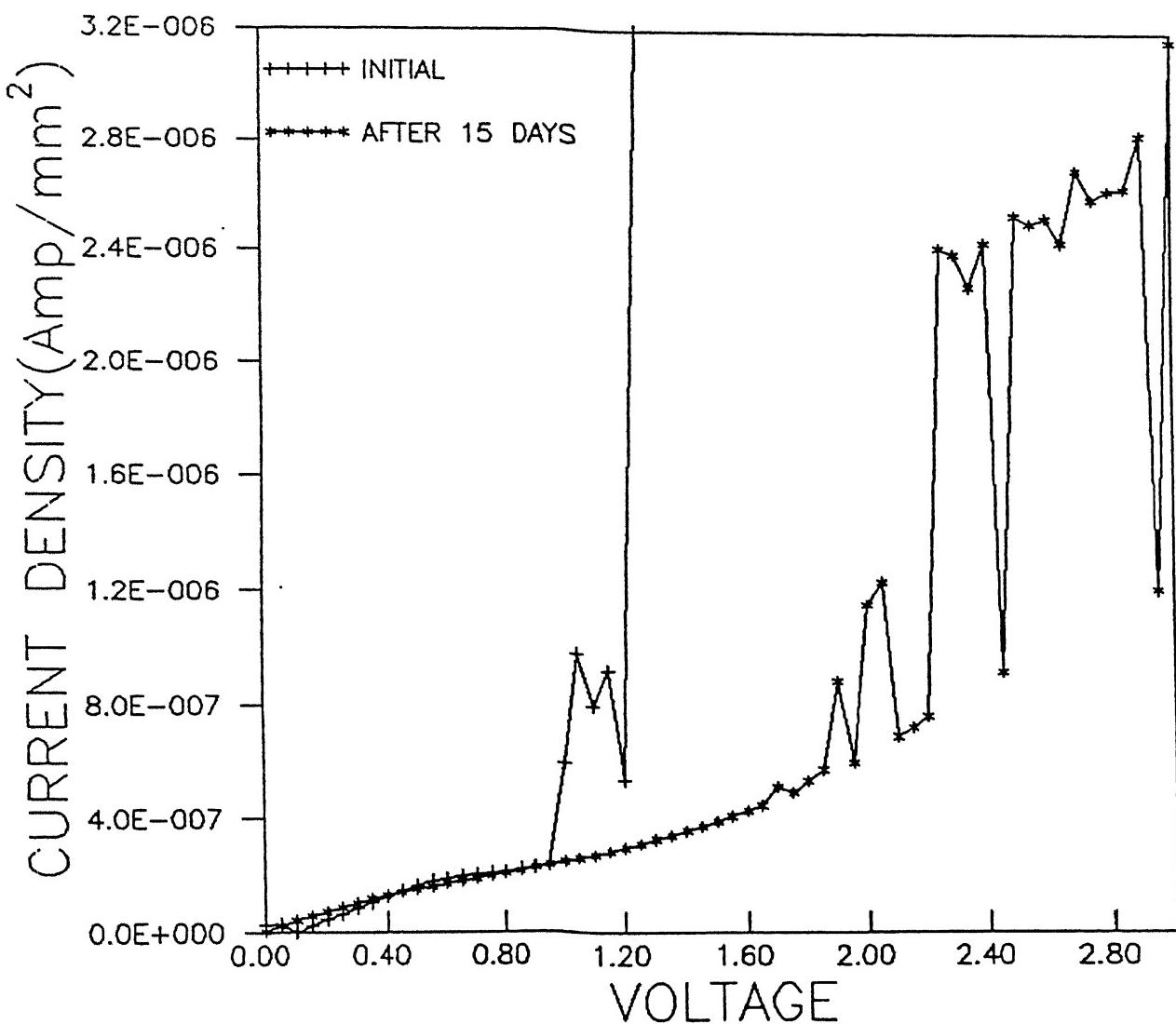
Fig.3.12 The J-V characteristics of a sample having oxide
grown at 100°C and junction area of 0.72mm² as
such and after 15 days of ageing.
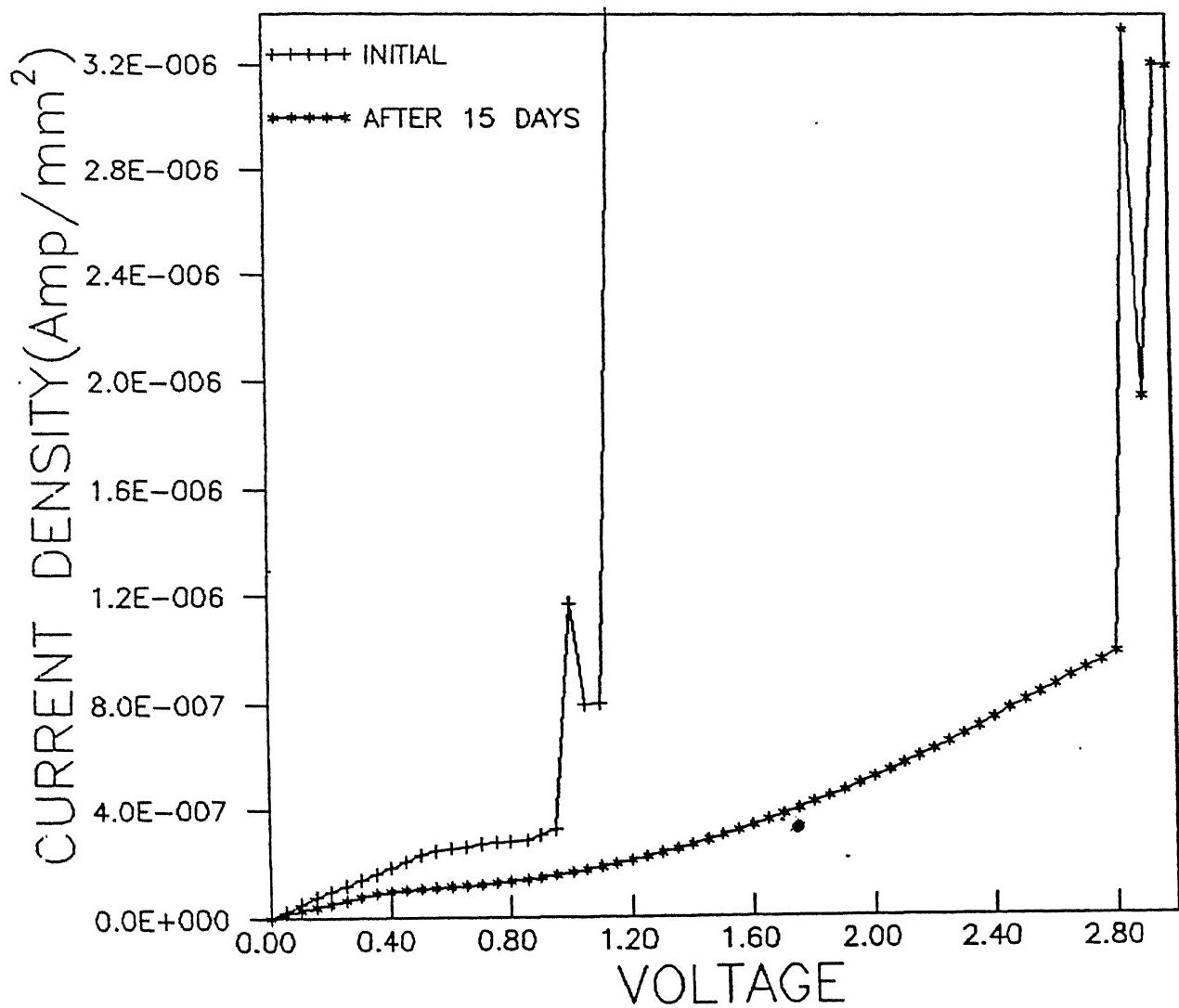
Fig.3.13 The J-V characteristics of a sample having oxide grown at $100^{\circ}$C and junction area of $2.1mm^2$ as such and after 15 days of ageing.

is explained on the basis of collision ionisation as well. The conduction electron gain energy from applied electric field (E) and transfer that to the bulk. The rate of gain and loss of energy remains equal only up to a critical electric field (Ec), above which, balance is disturbed and the so called intrinsic breakdown occurs. After the breakdown, original characteristics of the insulator reappears on the application of reverse voltage or by keeping $Al-Al_2O_3-Al$ junction for a few days [15]. This phenomenon is called recovery or ageing. Figs 3.11-3.13 show the J-V characteristics of a typical $Al-Al_2O_3-Al$ junction prior to and after subjecting to 15 days of ageing. Clearly, the current initially increases steadily and eventually shoots up (Fig.3.11). Alternatively, the current-voltage (J-V) characteristics exhibit voltage controlled negative resistance (VCNR) effects or forming prior to breakdown (Fig.3.12,3.13). The recovery of properties after ageing is not complete (evident from Fig. 3.11) as the current increases more slowly with voltage after 15 days, though the curve remains smooth upto 3V with no breakdown. This indicates improvement in the stability of the insulator. In other cases,however, current either retraces the same path (Fig.3.12)or corresponds to lower values (Fig.3.13) with VCNR emerging at much higher voltages, e.g., 1.9 and 2.8V following breakdown and 15 days of ageing. The phenomenon of VCNR (termed as "forming") is known to occur easily in non-stoichiometric insulators [37].

# CONCLUSIONS

$Al-Al_2O_3-Al$ thin film structures, having intermediate oxide grown thermally in air at 50, 100, 150 and $200^\circ C$ for 24h each, exhibit mainly Ohmic, Schottky emission and field assisted tunneling processes of conduction at low, intermediate and high voltage ranges, respectively. This description is valid at all the temperatures (viz., 25, 40 and $60^\circ C$). However, Ohmic range shrinks and Schottky emission and field assisted tunneling get initiated progressively at lower voltages with increase in temperature. Schottky barrier height $(\phi_o)$ and its lowering coefficient $(\beta s)$ are found to respectively decrease and increase with rise in temperature; their room temperature values being 0.704 eV and 0.055 $V^{1/2}$, respectively.

The measured capacitance $(Cm)$ is significantly influenced by the interfacial effects. It decreases with increase in temperature mainly due to the changes occurring in the interfacial capacitance despite the marginal increase of the bulk capacitance of $Al_2O_3$ with temperature. The changes can be attributed to the removal of the charges present at the interface.

The breakdown of $Al_2O_3$ occurs via rapid increase of current beyond a certain voltage or through a forming process distinguished by a voltage controlled negative resistance (VCNR) phenomenon. At this stage, the oxides turned fully conducting possibly

due to channels created in the bulk. Consequently, substantial heating takes place. The oxide becomes homogeneous and is able to relax by relieving the internal stress. Ageing of $Al-Al_2O_3-Al$ structure following breakdown results in recovery of the insulating properties of $Al_2O_3$. The samples now display VCNR/breakdown at much higher voltages. Obviously, $Al_2O_3$ becomes quite stable after the recovery presumably due to heating by heavy passage of current just before the breakdown.

# REFERENCES

1   H. Beiderman, *vacuum*, 26 (1976) 513.

2   Y. Nakamura, D.L. Klein and J.S.Tsai, *App Phys.Lett.*, 68 (1996) 275.

3   E. Murphy and R.H. Good, *Phys. Rev.* 102 (1956) 1464.

4   R. Holm, *J. Appl. Phys.*, 22 (1951) 569.

5   R. Stratton, *J. Appl. Phys. and chem. of Solids*, 23 (1962) 1177

6   S.R. Pollack and C.E. Morris, *J. Appl. Phys.*, 35 (1964) 1503.

7   J.G. Simmons, *J. Appl. Phys.*, 34 (1963) 2581.

8   C.M. Vodenicharov and S.G. Christov, *Solid state electronics* 15 (1972) 933.

9   D.V. Gepert, *J. Appl. Phys.* , 34 (1963) 490.

10  C.A. Mead, *J. Appl. phys.*, 32 (1962) 646.

11  E.I. Maissel and H. Glang (eds.), *Handbook of Thin Films Technolozy*, Mc Graw Hill, New York, 1970.

12  T.W. Hickmott, *J. appl. Phys.*, 32 (1962) 2669.

13  G. Dearnley, A.H. Stoneham and D.V. Morgan, *Rep. Prog. Phys.* 33 (1970) 1129.

14  H. Birey, *J. App. Phys.* , 48 (1977) 5209.

15  A.K. Ray and C.A. Hogarth, *Int. J. Elec.* , 57 (1984) 1.

16  L. Vijayraghwan, *Electrical Characteristics Of Thermally Grown $Al_2O_3$ Films*, M.Tech. Thesis, Indian Institute Of Technology, Kanpur (1990).

17  Anand Madhukar, *Current Voltage Characteristics Of $Al-Al_2O_3-Al$ structures*, M.Tech. Thesis, Indian Institute Of Technology, Kanpur (1996).

18    D.R. Lamb , *Electrical Conduction Mechanisms in Thin Insulating Films*, Hirst Research Centre, Wembley , 1967.

19    S.R. Pollack and J.A. Seitchik, *App. Solid State Science*, Vol1 R. Wolfe and Krissmen (eds.) Academic Press, New York,1969.

20    J.G. Simmons, *J. Appl. Phys.*, 35 (1963) 1793.

21    J.G. Simmons , *J. Appl. Phys*, 35 (1964) 2472.

22    J.G. Simmons, *Phys. Rev. Lett.*, 15 (1965) 967.

23    P.R. Emptage and W. Tantraporn, *Phys. Rev.Lett.*, 8 (1962) 267.

24    S.R. Pollack , *J. Appl. Phys.*, 34 (1963) 877.

25    D.A. Vermilyea, *Acta Metallurgica*, 2 (1954) 346.

26    J.G. Simmons, *Phys. Rev.*, 155 (1967) 657.

27    C.A. Mead, *Phys. Rev.*, 128 (1962) 2088.

28    N.F. Mott and R.W. Gurney, *Electronic Process in Ionic Solids*, Oxford University Press, Newyork, 1940.

29    A. Rose, *Phys. Rev.* ,97 (1955) 1538.

30    J.G. Simmons, In *Tunneling Phenomenon of In Solids*, E. Bustein and Lundquist (eds.), Plenum Press, Newyork (1969) 135.

31    A. Rahman and M.S. Raven, *Thin Solid Films*, 71 (1980) 7.

32    T.W. Hickmott , *Thin Solid Films*, 9 (1972) 431.

33    R.A. collins, G. Bowman and R.R. Sutherland, *J.Phys. D.*, 4 (1971) L 49.

34    N. Klein and Gafni, *IEEE Trans. Electron Devices*, ED 13 (1966) 281.

35    N. Klein and N. Levanon, *J. Appl. Phys.*,38 (1967) 3721.

36    J.C. Fisher and I. Giaever, *J. App. Phys.*, 32 (1961)172.

37    R.R. Verderber, J.G. Simmon s and B. Eales, *Phil. Mag.* ,1 (1967) 1049.

38  G. Deanley, D.V. Morgan and A.M. Stoneham *J. Non-Crystal. Solids*, 4 (1970) 593.

39  C. Barriac, *Phys. Stat. Solidi.*, 34 (1969) 621.

40  C.M. Vodenicherov and S.G. Christov, Solid State Electronics, 15 (1972) 933 ; *Phys. Stst. Solidi.* (a) 25 (1974) 387.

41  A.R. Bardhan, P.C. Srivastava, I.B. Bhattacharya and D.L. Bhattacharya, *Int. J. Elec.* , 39 (1975)343.

12  A.R. Bardhan, P.C. Srivastava, A. Chatterjee and D.L. Bhattacharya, *Int. J. Elec.*,40 (1976) 313.

43  S.P.S. Arya and H.P. Singh ,*Thin Solid Films*, 91 (1982) 363.

44. G. Blaise, *J. Appl. Phys.*, 77 (1995) 2916.

45  J. Harrop and D.S. Cambell, *in Handbook of Thin film Technology, E.I. Maissel and R. Glang (eds.), Macgraw Hill Newyork*, 1970 p 16-1.

46  L. Young, *Anodic Oxide Films*, Academic Press Newyork, 1961.

47  K.R. Lawless, *Rept. Prog. Phys.*, 37 (1974) 231.

48  J. Antula, *Phys. Stat. Solidi.* , 24 (1967) 89.

49  A.F. Hebard, S.A. Ajuria and R.H. Eick, *App. Phys. Lett.* 51(1987) 1349.

50  G.J. Hass, *J. opt. Soc. Amer.*, 39 (1949) 532.

51  H.Y. Ku and F.G. Ulman, *J. App. Phys.*, 32 (1964) 265.

52  J.G. Simmons , *App. Phys. Lett.* , 6 (1965) 54.

53  P.P. Bundestein, P.J. Hayes, J.L. Smith and W.B. Smith, *J. Vac. Sci. Tech*, 2 (1969) 289.

54  P.P. Bundestein and P.J. Hayes, *J. App. Phys.*, 38 (1967) 2837.